

# Higgs funnel region of SUSY dark matter for small $\tan\beta$ and renormalization group effects on pseudoscalar Higgs boson with scalar mass non-universality

Utpal Chattopadhyay and Debottam Das<sup>1</sup>

*Department of Theoretical Physics  
Indian Association for the Cultivation of Science  
2A and 2B Raja S.C. Mullick Road  
Jadavpur, Kolkata 700 032, India*

## Abstract

A non-universal scalar mass supergravity type of model is explored where the first two generation of scalars and the third generation of sleptons may be very massive. The lighter or vanishing third generation of squarks as well as Higgs scalars at the unification scale cause the radiative electroweak symmetry breaking constraint to be less prohibitive. Thus, both FCNC/CP-violation problems as well as the naturalness problem are within control. We identify a large slepton mass effect in the RGE of  $m_{H_D}^2$  (for the down type of Higgs) that may turn the later negative at the electroweak scale even for a small  $\tan\beta$ . A hyperbolic branch/focus point like effect is found for  $m_A^2$  that may result in very light Higgs spectra. The lightest stable particle is dominantly a bino that pair annihilates via Higgs exchange, giving rise to a WMAP satisfied relic density region for all  $\tan\beta$ . Detection prospects of such LSPs in the upcoming dark matter experiments both of direct and indirect types (photon flux) are interesting. The Higgs bosons and the third generation of squarks are light in this scenario and these may be easily probed besides charginos and neutralinos in the early runs of LHC.

PACS No: 04.65.+e, 13.40Em, 14.60Ef, 13.85.-t, 14.80.Ly

## 1 Introduction

Low energy supersymmetry (SUSY) [1] is one of the most active fields of research for physics beyond the standard model (SM) [2]. A minimal extension of the Standard Model when

---

<sup>1</sup>Emails: tpuc@iacs.res.in, tpdd@iacs.res.in

supersymmetry is incorporated is the Minimal Supersymmetric Standard Model (MSSM) [1, 3] that includes two Higgs doublets. The model however has a large number of SUSY breaking parameters and this motivates one into studying models with specific mechanisms for breaking SUSY. The later involves high scale physics input and renormalization group analyses. This in general leads to a large reduction of the number of unknown parameters. The minimal supergravity (mSUGRA) [4] model is one of the well studied SUSY models. It requires a very few input parameters at the gauge coupling unification scale or grand unified theory (GUT) scale,  $M_G \simeq 2 \times 10^{16}$  GeV. The parameters indeed quantify our ignorance of the exact nature of SUSY breaking. The model incorporates radiative breaking of electroweak symmetry (REWSB). The unification scale universal input parameters are: i) the gaugino mass parameter  $m_{\frac{1}{2}}$ , ii) the scalar mass parameter  $m_0$  and iii) the tri-linear SUSY breaking parameter  $A_0$ . Additionally, one has to provide with  $\tan\beta$ , the ratio of Higgs vacuum expectation values and the sign of the Higgsino mixing parameter  $\mu$ . Renormalization group evolutions are used to obtain the electroweak scale parameters of MSSM.

There is however no *a priori* necessity of considering such universalities of parameters. Indeed, it is worthwhile to explore scenarios with non-universalities in the scalar or in the gaugino masses at the unification scale [5–11]. Non-universal scalar masses may appear because of non-flat Kähler potential [12]. However, one must be careful to accommodate the stringent constraints from phenomena involving flavor changing neutral currents (FCNC). Satisfying FCNC constraints demands near-degeneracy of the first two generations of scalar masses but the requirements on the third generation of scalars as well as the Higgs scalars are not so stringent [13,14]. Thus it is seen that FCNC constraints as well as constraints from CP-violating phases (for example, those arising from the electric dipole moments of the electron and neutron) may be managed by introducing multi-TeV scalar masses for the first two generations of scalars [15]. The third generations of scalar masses and the Higgs scalar masses however should be adequately light in order to satisfy naturalness [16]. There have been several efforts for obtaining the desired features as outlined above. Analyses with Radiatively Generated Inverted Mass Hierarchy Models (RIMH) were made in Ref. [14,17,18]. In Ref. [18] the authors achieved the above-mentioned requirements at the electroweak scale by using  $t-b-\tau$  Yukawa unification with special non-universal relationship among the scalar masses at  $M_G$ . Here, the Higgs and the third generation of scalar masses are rapidly diminished at the electroweak scale via RG evolutions. However, the Yukawa unification and the consideration

of REWSB constrain such models heavily. A second realization of the above idea is partially possible via the hyperbolic branch (HB)/ focus point (FP) [19,20] scenarios where the scalars may become considerably massive (multi-TeV) in a subset of the typical mSUGRA parameter space satisfying universal boundary conditions while fine-tuning [16] still remains small. A third possibility was considered in Ref. [21], where plain decoupling arguments motivated the authors in using explicit splitting at  $M_G$  between the scalars belonging to the first two generations and the same of the third generation (along with the Higgs scalars). Here the first two generations of scalars were chosen in the multi-TeV domain whereas the third generation of scalars as well as the Higgs scalars were considered to be in the sub-TeV zone. Additionally, a large value of the tri-linear coupling parameter was chosen in Ref. [21] for the first two-generations. Universality of scalar masses in the first two-generations along with a choice of a different scalar mass parameter for the third generation as well as the Higgs scalars, or even splitting of squarks and sleptons within the third generation itself have also been considered in Refs. [22–24]. In Ref. [23] the authors additionally considered non-universality in the gaugino masses and analyzed the fine-tuning aspect of computing the relic density of dark matter in addition to obtaining a parameter zone of the MSSM corresponding to a well tempered neutralino [25]. Similarly, analyses with only non-universalities in the Higgs scalar may be seen in Refs. [6, 8, 10, 26]. A comprehensive set of characteristic possibilities for varieties of non-universal SUGRA scenarios may be seen in Ref. [27].

In this analysis we explore a SUGRA scenario with non-universal scalar masses that i) allows to have very large first two-generation of scalar masses so as to obey the FCNC and the CP-violation limits easily (*ie.* without requiring any ultra-small phases) and that would not impose any additional price on fine-tuning, ii) spans a large amount of MSSM parameter space satisfying the neutralino relic density constraint from WMAP data by not requiring any delicate mixing of bino and Higgsinos, so that we would find a bino-dominated lightest neutralino for most of the parameter space and, iii) satisfies the Higgs mass lower bound from LEP2 data as well as other low energy constraints. Certainly, a model with REWSB and universal scalar mass like mSUGRA is not friendly to achieve these objectives if we consider a common gaugino mass parameter below a TeV or so. The above phenomenologically inspired requirements in combination motivate us to introduce non-universality between the third and the first two-generation of scalars as well as the Higgs scalars. This has to be such that the REWSB conditions would not become prohibitive to have a multi-TeV first

two-generation of scalars. Here we would like to point out that we would not be able to satisfy the mentioned objectives by considering non-universalities only in the Higgs scalar masses.

A simpler and purely phenomenological attempt in this direction in a universal gaugino mass framework could be to generate all the third generation of scalar masses and the Higgs scalar masses radiatively, starting from zero values at the unification scale, while keeping the first two-generations of scalar masses universal (and this may be in the multi-TeV zone). We point out that starting with a similar range of values for the Higgs scalars as with the third generation of scalars at  $M_G$  would be desirable since this would lead to similar range of mass values for all the soft-SUSY breaking terms contributing to REWSB after RG evolutions. However, if we consider all the third generation of scalars at  $M_G$  to be light, we would find stau ( $\tilde{\tau}$ ) becoming the lightest stable particle (LSP) or even tachyonic at the electroweak scale. On a similar note, we remind that such an appearance of tachyonic sleptons also arise in the Anomaly Mediated Supersymmetry Breaking (AMSB) analyses, and it is avoided purely by a phenomenologically inspired way of adding an appropriate non-zero mass value to all the scalars at the unification scale in the minimal AMSB scenario [28]. Thus with a simple motivation of managing with FCNC and CP-violation, naturalness as well as the dark matter constraints concurrently we consider a non-zero mass value for the third generation of sleptons, while having the masses of squarks of the third generation and the Higgs scalars vanishing at  $M_G$ . Additionally, for convenience we set the third generation of slepton mass parameters the same as that of the first two-generation of scalars at  $M_G$ .

Thus, the parameters of our Non-universal Scalar Mass model which will henceforth be called the NUSM model is given by

$$\tan \beta, m_{\frac{1}{2}}, A_0, \text{sign}(\mu), \text{ and } m_0 \tag{1}$$

where the scalar mass input assignments at  $M_G$  are as follows.

- i) The unification scale mass parameter for the first two-generations of squarks, sleptons and the third generation of sleptons is  $m_0$ , where  $m_0$  is allowed to span up to a very large value.
- ii) The mass parameters for the third generation of squarks and Higgs scalars are set to zero. We could have also chosen a non-vanishing value for ii) as long as it is sufficiently small. We may note here that different values of mass parameters for squarks and sleptons at  $M_G$  may appear in orbifold models with large threshold corrections. This is related to having different modular weights associated with the squarks and the sleptons in a given generation [29, 30].

As we will see below, the NUSM model provides with a highly bino-dominated neutralino dark matter over almost its full range of parameter space. It has an interesting feature of having a large funnel region, a region of parameter space where the associated annihilation channels are characterized by the direct channel pole  $2m_{\tilde{\chi}_1^0} \simeq m_A, m_H$ . We note that unlike mSUGRA where one finds the funnel region only for a large value of  $\tan\beta$ , here in the NUSM one finds it for almost all possible values of  $\tan\beta (\gtrsim 5)$ . We will also see that the NUSM is further characterized by a lighter  $m_A$  or  $m_H$  particularly when  $m_0$  is large and this is found even for small values of  $\tan\beta (\sim 10)$ . A small part of the parameter space may be far from the decoupling [31] region of Higgs boson mixing that causes the lighter CP-even Higgs boson ( $h$ -boson) to be non-Standard Model like [32]. This in turn reduces the lower bound of  $m_h$  much below the LEP2 Higgs boson mass limit.

In this work we include a semi-analytic calculation that first points out a large mass effect in the solution of the renormalization group equations (RGE) of  $m_{H_D}^2$ . The effect causes a hyperbolic branch/focus point like behavior<sup>2</sup> in  $m_A^2 (\simeq m_{H_D}^2 - m_{H_U}^2)$  that may cause  $m_A$  to become smaller even for a small  $\tan\beta$  as mentioned above. Here we remind that  $m_A$  typically becomes smaller in mSUGRA only for large  $\tan\beta$ .

The paper is organized as follows. In Sec.2 we will primarily discuss the large mass RGE effects in the NUSM on  $m_A^2$  and its consequent reduction for large  $m_0$  via an HB/FP-like effect. We will obtain the semi-analytic results which will also be verified by numerical computation. In Sec.3 we will study the cold dark matter constraint from WMAP data including also the constraints from the LEP2 Higgs bound,  $b \rightarrow s + \gamma$ , and  $B_s \rightarrow \mu^+ \mu^-$ . We will also discuss a few sample points in the context of LHC reach. In Sec.4 we will discuss the direct and indirect detection (via continuous gamma ray) rates of the LSP. Finally we will conclude in Sec.5.

## 2 The non-universal scalar scenario:NUSM

In this section we focus on the key elements that are important for the NUSM. The primary quantities of phenomenological interest are  $\mu$ , and  $m_A$ . These in turn have important signif-

---

<sup>2</sup>We remind that the well known HB/FP effect that occurs in  $m_{H_U}^2$  is associated with the first minimization condition of Radiative electroweak symmetry breaking. In this analysis we do not have such an effect. On the contrary we have a similar HB/FP effect for small values of  $\tan\beta$  in connection with the second minimization condition that is associated with  $m_A^2$ .

icance on the following: i) the issue of fine-tuning, ii) the presence of non-Standard Model like lighter Higgs boson mass bound for a limited region of parameter space, iii) dark matter and iv) collider discovery possibilities. Additionally, we remind ourselves about obtaining a lighter third generation of squarks at the electroweak scale and this is of course related to their vanishing values at the unification scale.

To start with we write down the REWSB results,

$$\mu^2 = -\frac{1}{2}M_Z^2 + \frac{m_{H_D}^2 - m_{H_U}^2 \tan^2 \beta}{\tan^2 \beta - 1} + \frac{\Sigma_1 - \Sigma_2 \tan^2 \beta}{\tan^2 \beta - 1}, \quad (2)$$

and,

$$\sin 2\beta = 2B\mu/(m_{H_D}^2 + m_{H_U}^2 + 2\mu^2 + \Sigma_1 + \Sigma_2) \quad (3)$$

where  $\Sigma_{1,2}$  represent the one-loop corrections [33, 34], that become small in the scale where the Higgs potential  $V_{Higgs}$  is minimized. We may approximately consider  $\mu^2 \simeq -m_{H_U}^2$  (for  $\tan \beta \gtrsim 5$ ) and  $m_A^2 = m_{H_D}^2 + m_{H_U}^2 + 2\mu^2 \simeq m_{H_D}^2 - m_{H_U}^2$  at tree level.

The associated one-loop RGEs are given by (neglecting the very small first two-generations of Yukawa contributions),

$$\begin{aligned} \frac{dm_{H_D}^2}{dt} &= (3\tilde{\alpha}_2\tilde{m}_2^2 + \frac{3}{5}\tilde{\alpha}_1\tilde{m}_1^2) - 3Y_b(m_{H_D}^2 + m_Q^2 + m_D^2 + A_b^2) \\ &\quad - Y_\tau(m_{H_D}^2 + m_L^2 + m_E^2 + A_\tau^2) + \frac{3}{10}\tilde{\alpha}_1 S_0 \end{aligned} \quad (4)$$

$$\frac{dm_{H_U}^2}{dt} = (3\tilde{\alpha}_2\tilde{m}_2^2 + \frac{3}{5}\tilde{\alpha}_1\tilde{m}_1^2) - 3Y_t(m_{H_U}^2 + m_Q^2 + m_U^2 + A_t^2) - \frac{3}{10}\tilde{\alpha}_1 S_0 \quad (5)$$

Here we have  $t = \ln(M_G^2/Q^2)$  with  $Q$  being the renormalization scale.  $\tilde{\alpha}_i = \alpha_i/(4\pi)$  for  $i = 1, 2, 3$  are the scaled gauge coupling constants (with  $\alpha_1 = \frac{5}{3}\alpha_Y$ ) and  $\tilde{m}_i$  are the running gaugino masses, where  $i = 1, 2, 3$  refers to U(1), SU(2) and SU(3) gauge groups respectively.  $Y_j$  represent the scaled and squared Yukawa couplings, e.g,  $Y_j \equiv h_j^2/(4\pi)^2$  where  $h_j$  is a Yukawa coupling ( $j = 1, 2, 3$  stands for  $t, b, \tau$  respectively). The quantity  $S_0$  which is shown below may become relevant for a general set of non-universal boundary condition for scalars. However in this analysis it is zero at  $M_G$  and it causes only a negligible effect.

$$S_0 = m_{H_U}^2 - m_{H_D}^2 + \Sigma_k(m_{q_k}^2 + m_{d_k}^2 + m_{e_k}^2 - m_{l_k}^2 - 2m_{\bar{u}_k}^2) + (m_Q^2 + m_D^2 + m_E^2 - m_L^2 - 2m_U^2) \quad (6)$$

where the subscript  $k$  for  $k = 1$  or  $2$  indicates the first two generations.

The solutions for  $\mu^2$  and  $m_A^2$  valid up to a moderately large value of  $\tan\beta$  (10 or so) follow from Ref. [6] after appropriately considering the NUSM parameters. This involves ignoring  $h_b$  and  $h_\tau$  in the limit of a small  $\tan\beta$ . The solutions read

$$\mu^2 = m_0^2 C_1 + A_0^2 C_2 + m_{\frac{1}{2}}^2 C_3 + m_{\frac{1}{2}} A_0 C_4 - \frac{1}{2} M_Z^2 + \frac{3 \tan^2 \beta + 1}{5 \tan^2 \beta - 1} S_0 p, \quad \text{and} \quad (7)$$

$$m_A^2 = m_0^2 D_1 + A_0^2 D_2 + m_{\frac{1}{2}}^2 D_3 + m_{\frac{1}{2}} A_0 D_4 - \frac{1}{2} M_Z^2 + \frac{6 \tan^2 \beta + 1}{5 \tan^2 \beta - 1} S_0 p. \quad (8)$$

Here  $p$  is given by:  $p = \frac{5}{66}[1 - (\frac{\tilde{\alpha}_1(t)}{\tilde{\alpha}_1(0)})]$ . The unification scale conditions for scalar mass squares for the NUSM may be given as  $m_i^2 = (1 + \delta_i)m_0^2$ . Here, the subscript  $i$  for  $\delta_i$  stands for:  $i \equiv H_D, H_U, Q_L, u_R, d_R, l_L, e_R$ . For NUSM one has  $\delta_{H_u} = \delta_{H_D} = \delta_{Q_L} = \delta_{u_R} = \delta_{d_R} = -1$  and  $\delta_{l_L} = \delta_{e_R} = 0$ . These unification scale conditions allow us to define a quantity  $\delta$  that appears in the expressions of the coefficients  $C_1$  and  $D_1$  as shown below. It follows that  $\delta = -1$  for the NUSM, and  $\delta = 0$  for mSUGRA. We note that only  $C_1$  among  $C_i$ 's and  $D_1$  among  $D_i$ 's depend on  $\delta$  and one obtains<sup>3</sup>,

$$\begin{aligned} C_1 &= (1 + \delta) \frac{1}{\tan^2 \beta - 1} \left(1 - \frac{3D_0 - 1}{2} \tan^2 \beta\right), \quad \text{and} \\ D_1 &= \frac{3}{2} (1 + \delta) \frac{\tan^2 \beta + 1}{\tan^2 \beta - 1} (1 - D_0). \end{aligned} \quad (9)$$

Here,  $D_0 \simeq 1 - (m_t/200 \sin\beta)^2 \lesssim 0.2$ . The definitions of the quantities  $C_i$  and  $D_i$  for  $i \neq 1$  may be seen in the appendix. As mentioned above, for the NUSM one has  $\delta = -1$ . Hence, Eqs. 7-9 show that at the level of approximation where  $h_b$  and  $h_\tau$  are ignored,  $\mu^2$  and  $m_A^2$  are independent of  $m_0$ . We will however see that both  $\mu^2$  and  $m_A^2$  would actually depend on  $m_0$ . While the dependence of  $\mu^2$  on  $m_0$  would be caused by two-loop RGE effects in  $m_{H_U}^2$ , the same for  $m_A^2$  is very prominent even at the one-loop level of RGE and this is found when we include the effects due to  $h_b$  and  $h_\tau$  which are specially important for the NUSM. The following subsection describes our improved results.

---

<sup>3</sup>In Ref. [6] the authors considered non-universalities in the masses of Higgs scalars and the third generation scalars  $m_{Q_L}$  and  $m_{u_R}$ . However, NUSM additionally requires non-universality in  $m_{d_R}$ .

## 2.1 Large slepton mass RGE effect on pseudoscalar Higgs boson– A hyperbolic branch/focus point like effect in $m_A^2$ for small $\tan\beta$

Numerical computation shows that unlike what is seen from Eqs. 8 and 9,  $m_A^2$  may indeed decrease very rapidly with an increase of  $m_0$  for large values of the later. There are two reasons behind the above behavior: i) the choice of vanishing Higgs scalars in the NUSM at the unification scale  $M_G$  and ii) a large slepton mass (LSM) effect in the RGE of Eq.4 via the tau-Yukawa term. Henceforth, we will refer the combined effect of i) and ii) as the LSM effect. In this analysis we first compute  $m_{H_D}^2$  analytically without ignoring the terms involving  $h_b$  and  $h_\tau$ . The calculation essentially keeps the terms involving the bottom and the tau-Yukawa couplings similar to what was used for the top-Yukawa term of Eq.4 in Refs. [6, 35]. This results into,

$$m_{H_D}^2 = C_{H_D} m_0^2 + m_{1/2}^2 g(t) + \frac{3}{5} S_0 p. \quad (10)$$

Here  $g(t)$  is a function of  $\tan\beta$  [35]. The term involving  $S_0$  vanishes in the NUSM. At the level of approximation where the bottom and tau Yukawa couplings are straightway ignored in Eq.4,  $C_{H_D}$  would become zero in the NUSM. The result of our computation of  $C_{H_D}$  that leads to a non-vanishing value is given below.

$$C_{H_D} = C_{H_D}(U) + C_{H_D}(NU) \quad (11)$$

where,

$$\begin{aligned} C_{H_D}(U) &= 1 - 3(3I_2 + I_3) \\ C_{H_D}(NU) &= \delta_{H_D} - 3I_2(\delta_{Q_L} + \delta_{d_R} + \delta_{H_D}) \\ &\quad - I_3(\delta_{l_L} + \delta_{e_R} + \delta_{H_D}). \end{aligned} \quad (12)$$

The quantities  $I_2$  and  $I_3$  are functions of  $Y_i = \frac{h_i^2}{(4\pi)^2}$  for  $i = 2, 3$  ( $b, \tau$ ). Small  $\tan\beta$  solutions of  $Y_i$ s, computed at the electroweak scale [35] are shown in the appendix.  $I_2$  and  $I_3$  defined below are computed numerically.

$$I_2 = \int_0^t Y_2(t') dt', \quad I_3 = \int_0^t Y_3(t') dt' \quad (13)$$

Here  $t = \ln(M_G^2/M_Z^2)$ . One finds  $I_2, I_3 \ll 1$ . For NUSM, the above reduces to

$$C_{H_D} = -2I_3. \quad (14)$$



Since  $I_3$  is proportional to the square of  $\tau$ -Yukawa coupling  $h_\tau$  where  $h_\tau \propto \frac{1}{\cos\beta}$ , we find  $|C_{H_D}|$  to be an increasing function of  $\tan\beta$ . For  $\tan\beta = 10$ , we find  $C_{H_D} \simeq -0.007$ . The above clearly shows the large slepton mass effect because the dependence of  $C_{H_D}$  or  $m_{H_D}^2$  on  $I_3$  arises from the term of Eq.4 that is associated with  $h_\tau^2$ . Thus with the NUSM parameters, the scalar mass term that appears as the first term in Eq.10 is essentially contributed by the third generation of slepton masses. Eq.10 and Eq.14 clearly show that even with a small  $\tan\beta$ , larger values of  $m_0$  may reduce  $m_{H_D}^2$  appreciably and may turn the later negative. This demonstrates the LSM effect as mentioned before<sup>4</sup>. We are not aware of any past reference that pointed out this large mass effect or provided with semi-analytic expressions. For larger  $\tan\beta$ ,  $C_{H_D}$  may be appreciably large and negative that causes the LSM effect to become prominent even for a smaller value of  $m_0$ .

We note that there is no LSM effect that may modify  $\mu^2$  of Eq.7 at the one-loop level. This is simply because  $\mu^2 \simeq -m_{H_U}^2$  and there is no possibility of having a LSM effect in the corresponding RGE of Eq.5. On the other hand, an improved  $m_{H_D}^2$  as obtained above in Eqs.10 and 14 changes the result of  $m_A^2$  (Eq.8 and 9) but the later does not receive any additional  $m_0^2$  dependence other than what is already contributed from Eq.14. Thus it follows that the coefficient of  $m_0^2$  when Eq.8 is modified would be  $C_{H_D}$ . As a result, in the above analysis that is valid for small  $\tan\beta$  below 10 or 15, we find that the LSM effect causes  $m_A^2$  to have a HB/FP like behavior for its dependence on  $m_0$  and  $m_{\frac{1}{2}}$ . Hence,  $m_A$  may become significantly small for a large  $m_0$  because of a cancellation between the terms. This of course may happen even for a small value of  $\tan\beta$ . A very large  $m_0$  would cause  $m_A^2$  to become tachyonic, or would result into an absence of REWSB (Eq.3). For a large  $\tan\beta$  on the other hand, the LSM effect is drastically enhanced. We comment here that in spite of showing the one-loop results we performed a complete numerical solution of the RGEs up to two loops in this analysis using SUSPECT [36].

We now point out that a simple non-universal Higgs scalar mass scenario as described

---

<sup>4</sup>(i) We must mention that if we had chosen the values of Higgs scalar masses to be  $m_0$  at the unification scale, the resulting coefficient of  $m_0^2$  in  $m_{H_D}^2$  would be positive and the later would no longer be a decreasing function of  $m_0$ . (ii) We further note that the fact that the third generation of squark masses are vanishing in NUSM also makes the LSM effect prominent. For example, had we considered non-vanishing values for  $m_Q$  and  $m_D$  ( $= m_0$ , ie.  $\delta_{Q_L} = \delta_{d_R} = 0$ ) we would find the terms in Eq.12 that are associated with  $I_2$  to become more prominent. This would have caused  $m_{H_D}^2$  to be further negative. However, it could also cause  $m_Q^2$  to turn tachyonic at the electroweak scale. We have also checked this fact numerically.

in Ref. [10] may also provide a small  $m_A$  along with a funnel type of region that satisfies the WMAP data, for a smaller value of  $\tan\beta$ . We emphasize in particular the case where non-universality was analyzed with a unified Higgs scalar mass in Ref. [10]. However, unlike the NUSM these scenarios are very much constrained via REWSB so that considering larger values of masses for the first two-generation of scalars, an easier way to control FCNC and CP-violation effects is not possible. In these non-universal Higgs scalar models  $m_A$  becomes small for small values of  $\tan\beta$ , only when tachyonic values of  $m_{H_D}^2$  and  $m_{H_U}^2$  (assumed equal) are considered at the unification scale and this severely reduces the available parameter space. Additionally, one may obtain an  $A$ -pole annihilation region or a funnel region for a small value of  $\tan\beta$  in the so called sub-GUT CMSSM scenario [37].

We will now describe our results as obtained by using SUSPECT [36]. Fig.1 shows the variation of  $\mu$  and  $m_A$  when  $m_0$  is varied in the NUSM and mSUGRA. Fig.1(a) shows the effect of varying  $m_0$  in mSUGRA and in the NUSM for  $m_{1/2} = 500$  GeV and 1 TeV. A small reduction of  $|\mu|$  ((10 to 20%)) is seen in the NUSM when  $m_0$  is increased up to 5 or 10 TeV. The approximate one-loop result of Eq.7 and Eq.9 with  $\delta = -1$  as in NUSM however would indicate a flat  $\mu$  over a variation of  $m_0$ . The figure of course shows a moderately varying  $\mu$  and we have checked that this variation has its origin in two-loop RGE effects. The two different  $m_{1/2}$  contours for mSUGRA however show a decreasing behavior of  $\mu$  when  $m_0$  is enhanced. This happens simply because of the HB/FP effect existing in mSUGRA. Fig.1(b) shows the results for  $m_A$  which have two sets of contours for  $m_{1/2} = 500$  GeV and 1 TeV corresponding to mSUGRA and the NUSM. In contrast to mSUGRA where  $m_A$  rapidly increases with  $m_0$ , the behavior in NUSM is opposite so that we may find a very light pseudoscalar Higgs boson via the LSM effect. The decrease of  $m_A$  is even more pronounced for a large value of  $\tan\beta$  and this may be easily seen in Fig.1(c) where a variation of  $m_A$  vs  $m_0$  is shown for a given  $m_{1/2}(= 500$  GeV) for three different values of  $\tan\beta$ . The curves ends in the larger  $m_0$  sides for a few different reasons. For  $\tan\beta \lesssim 10$ , the largest  $m_0$  limit is caused by stop mass becoming very light or unphysical. On the other hand for  $\tan\beta \gtrsim 15$  the largest  $m_0$  limit is given by absence of REWSB (ie  $m_A^2$  turning negative).

The LSM effect may be explicitly seen in Fig.2 where we plot squared scalar masses of Higgs scalars as well as their difference  $m_A^2 \simeq m_{H_D}^2 - m_{H_U}^2$  with respect to a variation over the renormalization scale  $Q$  for mSUGRA and the NUSM for  $\tan\beta = 10$ ,  $m_{1/2} = 400$  GeV and  $A_0 = 0$ . Fig.2(a) corresponds to mSUGRA for  $m_0 = 1$  TeV whereas Fig.2(b) shows the

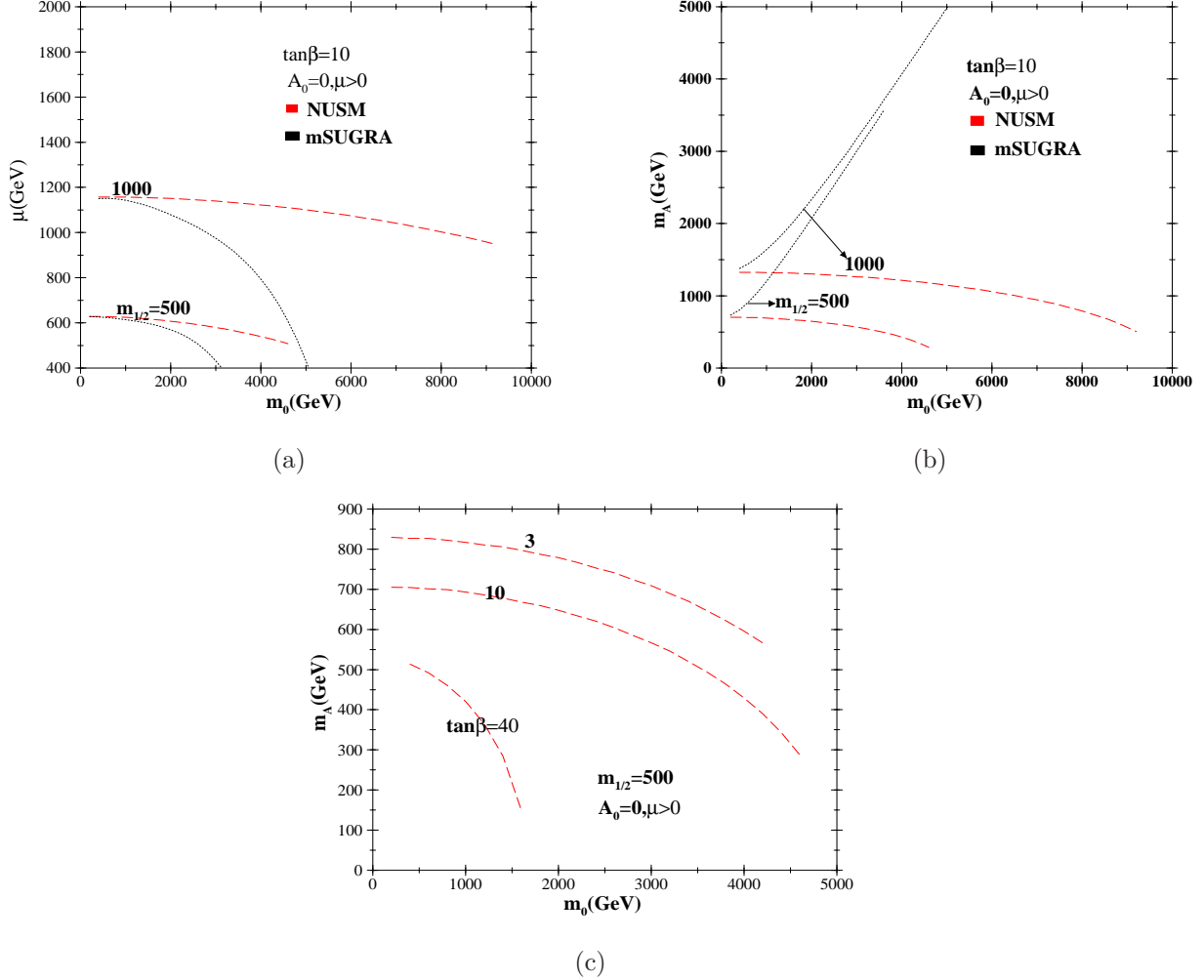


Figure 1: (a) Variation of  $\mu$  with  $m_0$  for  $\tan\beta = 10$ ,  $A_0 = 0$  and  $m_{\frac{1}{2}} = 500, 1000\text{GeV}$ . The red dashed lines represent the curves for the NUSM and the black dotted lines represent the same for mSUGRA. (b) Same as (a), but CP-odd Higgs ( $m_A$ ) is plotted against  $m_0$ . (c) shows the variation of  $m_A$  with  $m_0$  in the NUSM for different values of  $\tan\beta$  when  $m_{\frac{1}{2}} = 500\text{GeV}$ .

case of the NUSM for  $m_0 = 5\text{ TeV}$ . We have chosen different values of  $m_0$  in the two figures because of the fact that a large  $m_0$  is prohibited in mSUGRA via the REWSB constraint whereas a choice of a small  $m_0$  in the NUSM would have a negligible LSM effect. Clearly,  $m_{H_D}^2$  stays positive at the electroweak scale in mSUGRA (Fig.2(a)). On the other hand the same for the NUSM turns toward a negative value while running from  $M_G$  to the electroweak scale (Fig.2(b)) and this essentially shows the LSM effect in  $m_A^2$ . Thus a typical large  $\tan\beta$  phenomenon that occurs in mSUGRA is obtained in the NUSM for a small  $\tan\beta$ .

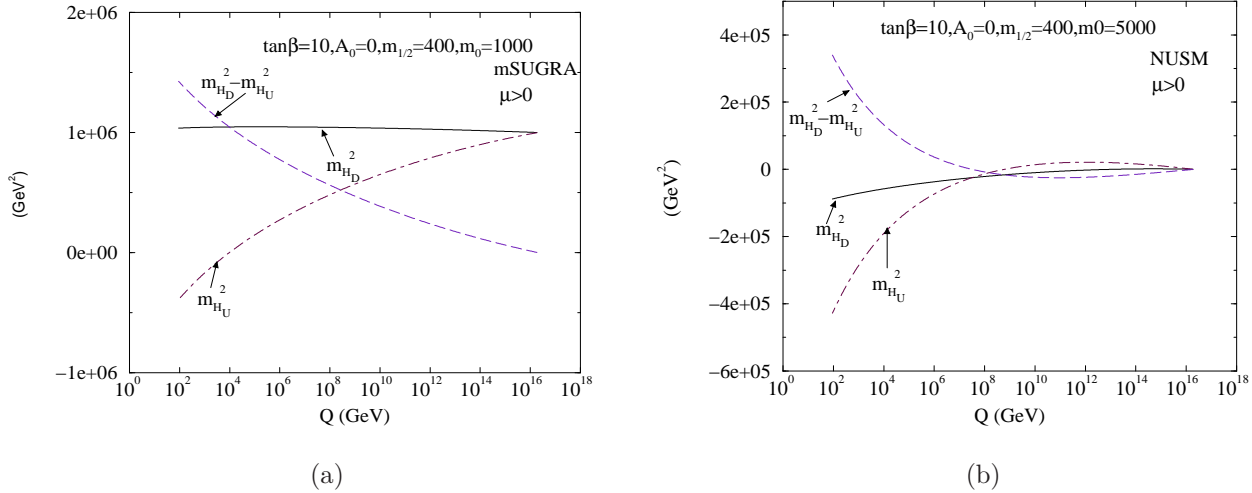


Figure 2: (a) Variation of squared Higgs scalar masses and their difference ( $\equiv m_A^2 \simeq m_{H_D}^2 - m_{H_U}^2$ ) with renormalization scale  $Q$  for  $\tan\beta = 10$ ,  $m_{\frac{1}{2}} = 400$  GeV,  $m_0 = 1000$  GeV and  $A_0 = 0$  for mSUGRA. (b) Same as (a), except for  $m_0 = 5000$  GeV and for the NUSM.  $m_{H_D}^2$  turns negative via LSM effect.

### 3 Cold dark matter constraint and extended funnel region

In supergravity type of models  $\tilde{\chi}_1^0$  becomes the LSP for most of the parameter space [38, 39] and we assume that the cold dark matter relic density is entirely due to  $\tilde{\chi}_1^0$ . Considering WMAP data [40] one finds a  $3\sigma$  limit as shown below.

$$0.091 < \Omega_{CDM} h^2 < 0.128 \quad (15)$$

where  $\Omega_{CDM} h^2$  is the DM relic density in units of the critical density. Here,  $h = 0.71 \pm 0.026$  is the Hubble constant in units of  $100 \text{ Km s}^{-1} \text{ Mpc}^{-1}$ . In the thermal description, the LSP was in thermal equilibrium with the annihilation products at a very high temperature of the early universe ( $T \gg m_{\tilde{\chi}_1^0}$ ). The annihilation products include fermion pairs, gauge boson pairs, Higgs boson pairs or gauge boson-Higgs boson combinations and they are produced via  $s, t$  and  $u$ -channel processes. As the temperature decreased the annihilation rate fell below the expansion rate of the universe and the LSP went away from the thermal equilibrium and freeze-out occurred. The current value of  $\Omega_{\tilde{\chi}_1^0} h^2$  is computed by solving the Boltzmann equation for  $n_{\tilde{\chi}_1^0}$ , the number density of the LSP in a Friedmann-Robertson-Walker universe. The above computation essentially involves finding the thermally averaged quantity

$\langle \sigma_{eff} v \rangle$ , where  $v$  is the relative velocity between two annihilating neutralinos and  $\sigma_{eff}$  is the neutralino annihilation cross section that includes all the final states. In addition to annihilations one considers coannihilations [41–45] which are annihilations of the LSP with sparticles close in mass values with that of the LSP. The cross section sensitively depends on the nature of the composition of the LSP. In the MSSM, the LSP is a mixed state of bino ( $\tilde{B}$ ), wino ( $\tilde{W}$ ) and Higgsinos ( $\tilde{H}_1^0$   $\tilde{H}_2^0$ ):

$$\tilde{\chi}_1^0 = N_{11}\tilde{B} + N_{12}\tilde{W}_3 + N_{13}\tilde{H}_1^0 + N_{14}\tilde{H}_2^0. \quad (16)$$

Here  $N_{ij}$  are the elements of the matrix that diagonalizes the neutralino mass matrix. The gaugino fraction  $F_G$  of the lightest neutralino is defined by  $F_g = |N_{11}|^2 + |N_{12}|^2$ . A gaugino-like LSP may be defined to have  $F_g$  very close to 1 ( $\gtrsim 0.9$ ). On the other side, a Higgsino-like LSP would have  $F_g \lesssim 0.1$ . For values in between, the LSP could be identified as a gaugino-higgsino mixed state. The MSSM with gaugino masses universal at  $M_G$  has a few distinct regions in general that satisfy the WMAP constraint. In this section we point out the existence of such regions in the context of the NUSM. i) The *bulk annihilation* region in mSUGRA is typically characterized by smaller scalar masses and smaller values of  $m_{1/2}$  where the LSP is bino-dominated. A bino dominated LSP couples favorably with right handed sleptons. Thus, the LSP pair annihilation in the bulk annihilation region occurs primarily via a t-channel sfermion in mSUGRA. There are two important constraints that disfavours the bulk region in mSUGRA. These are the constraints a) from the slepton mass lower limit from LEP2 [46] and b) from the lower limit of Higgs boson mass  $m_h$  of 114.4 GeV [47]<sup>5</sup>. ii) The *focus point* [19] or the *hyperbolic branch* [20] region of mSUGRA is typically characterized by a small  $|\mu|$  region that is close to the boundary of the lighter chargino mass lower bound. Because of a small  $|\mu|$  here the LSP has a significant amount of the Higgsino component or it can even be almost a pure Higgsino<sup>6</sup>. Additionally the lighter chargino  $\tilde{\chi}_1^\pm$  becomes lighter and coannihilations [43, 44] with LSP reduce the relic density to an acceptable level. The HB/FP region is however absent in the NUSM.

iii) Coannihilations of LSP may also occur with sleptons, typically staus ( $\tilde{\tau}_1$ ) [41] in mSUGRA. These regions are associated with small  $m_{1/2}$  and small  $m_0$  zones near the boundary of the discarded zone where staus become the LSP. Stau coannihilation is also an effective way to

---

<sup>5</sup>It is quite possible to have a bulk region with a non-zero  $A_0$  [48].

<sup>6</sup>This holds in the inversion region of the Hyperbolic branch [20].

bring the neutralino relic density to an acceptable level in the NUSM. Coannihilations of LSP may also occur with stop ( $\tilde{t}_1$ ) in a general MSSM scenario [42] or even in mSUGRA [48]. However, in spite of having relatively lighter  $\tilde{t}_1$ , the NUSM does not have such a region unless one reduces the mass of  $\tilde{t}_1$  further via appropriately considering non-zero values for  $A_0$ .

iv) The most important region satisfying WMAP data for our study is the Higgs-pole annihilation or *funnel* region [49, 50]. The funnel region that satisfies the WMAP data is characterized by the direct-channel pole  $2m_{\tilde{\chi}_1^0} \simeq m_A, m_H$ . This occurs in mSUGRA typically for large  $\tan\beta$  extending to larger  $m_0$  and larger  $m_{1/2}$  regions. In the NUSM however, the funnel region occurs in all possible  $\tan\beta$  ( $\gtrsim 5$ ). Indeed apart from the LSP-stau coannihilation appearing in a small region, Higgs-pole annihilation is the primary mechanism in the NUSM to satisfy the WMAP constraint throughout the parameter space.

We now show the results of the computation of the neutralino relic density using the code micrOMEGAs [51]. In Fig.3(a) that corresponds to  $\tan\beta = 10$  the region with red dots in the  $(m_{\frac{1}{2}} - m_0)$  plane satisfy the WMAP constraint (Eq.15) for the neutralino relic density. For a small  $m_0$  we find the stau coannihilation region marked with red dots. The gray region below the stau coannihilation region is discarded because of the appearance of charged LSPs.

The upper gray region is discarded broadly via  $m_A^2$  turning negative except near the boundary where there can be interplay with other constraints as described below. Thus if we concentrate on the boundary of the discarded region, the smallest  $m_{1/2}$  zone (below 160 GeV or so) is ruled out by the LEP2 lower limit of sparticle masses [46]. This is followed by obtaining tachyonic sfermion scalars (particularly stop scalars) when  $m_{\frac{1}{2}}$  is increased further up to  $\simeq 600$  GeV. The same boundary zone for the larger  $m_{1/2}$  region is eliminated because of the appearance of the charge and color breaking (CCB) minima [52]. In the NUSM this happens via the CCB conditions that involve  $m_{H_D}^2$ , the later becoming negative makes the CCB constraint stronger. In the region between the stau coannihilation area and the upper gray shaded discarded area one finds a long red region that satisfies the WMAP constraint for  $\Omega_{\tilde{\chi}_1^0} h^2$ . As mentioned before, the reason for satisfying the WMAP data is the direct channel annihilation of two LSPs via neutral Higgs bosons. Fig.3(b) shows a scanned output for  $\tan\beta = 10$  when  $m_0$  is varied as in Fig.3(a). The LSP mass is plotted against  $(2m_{\tilde{\chi}_1^0} - m_A)/2m_{\tilde{\chi}_1^0}$  so as to show the extent of the  $A$ -annihilation or funnel effect. Clearly the WMAP satisfied points shown in red fall around the zero of the y-axis confirming that the

funnel region appears in the NUSM for small  $\tan\beta$  as well. We note that the  $A$ -width can be quite large ( $\Gamma_A \sim 10\text{-}50$  GeV) and  $2m_{\tilde{\chi}_1^0}$  can be appreciably away from the exact resonance zone still giving a  $s$ -channel annihilation consistent with the WMAP data. The heavy scalar Higgs boson  $H$  also significantly contributes to the total annihilation cross-section. We now

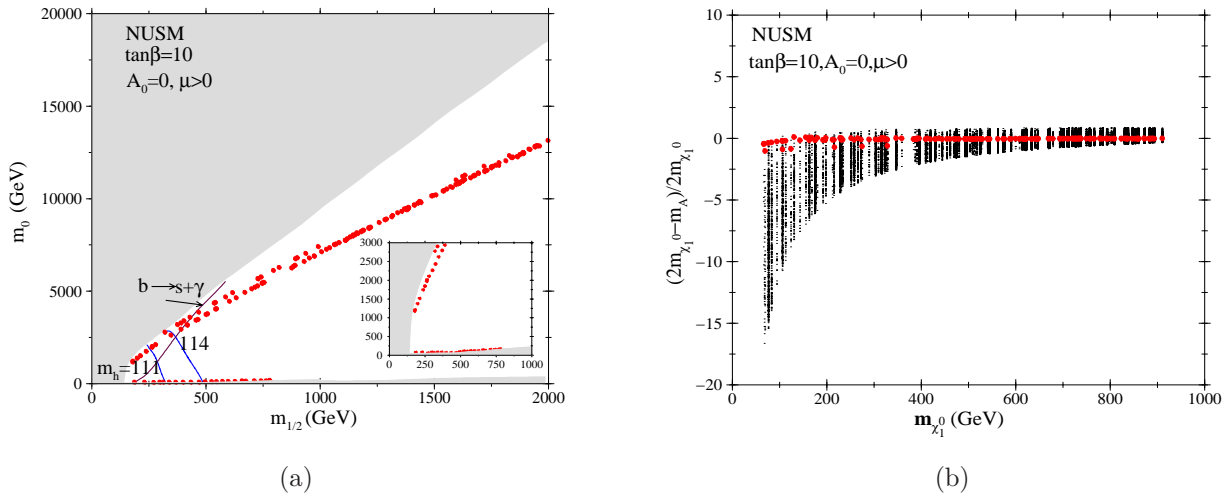


Figure 3: (a) WMAP allowed region in the  $m_{1/2} - m_0$  plane for  $\tan\beta = 10$  and  $A_0 = 0$  with  $\mu > 0$  for NUSM. Lighter Higgs boson mass limits are represented by solid lines. Dot-dashed line refers to  $b \rightarrow s\gamma$  limit. WMAP allowed regions are shown by red dots. The entire region is allowed via  $B_s \rightarrow \mu^+\mu^-$  bound. The small figure within the inset is shown for an improved display of the stau coannihilation zone. (b) Scattered points in the plane of  $m_{\tilde{\chi}_1^0}$  vs  $(2m_{\tilde{\chi}_1^0} - m_A)/2m_{\tilde{\chi}_1^0}$  shown after a scanning of  $m_{1/2}$  and  $m_0$  for  $\tan\beta = 10$ . Almost all the WMAP satisfied points (in red) occur near the zero of the y-axis, thus suggesting the  $s$ -channel annihilation of the LSPs via  $A$  and  $H$  bosons.

discuss the result of using a few constraints. First, we use the LEP2 limit [47] of 114.4 GeV for the SM Higgs boson. For the CP-even lighter SUSY Higgs boson mass  $m_h$  we use the same constraint as long as we are in the decoupling region [31] where the SUSY  $h$ -boson is SM-like. In the NUSM this is true for almost all the parameter space except a very small region with small  $m_{\frac{1}{2}}$  and for  $\tan\beta \gtrsim 15$  which we will discuss later. Additionally, we note that there is an uncertainty of about 3 GeV in computing the mass of the light Higgs boson [53]. This theoretical uncertainty primarily originates from momentum-independent as well as momentum-dependent two-loop corrections, higher loop corrections from the top-stop sector etc. Hence, we have drawn a contour for  $m_h = 111$  GeV in order to consider an

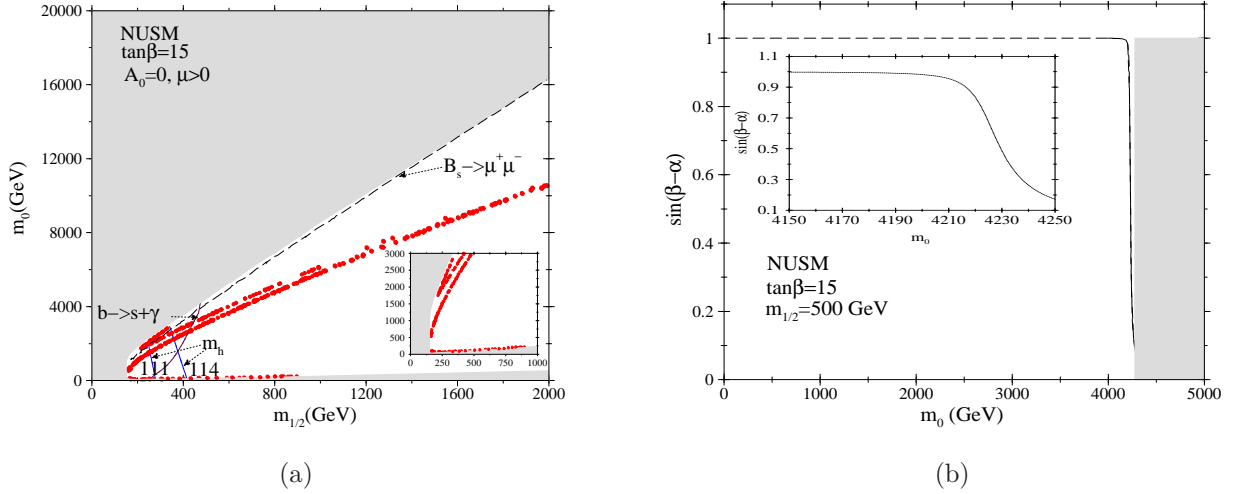


Figure 4: (a) WMAP allowed region in the  $m_{1/2} - m_0$  plane for  $\tan \beta = 15$  and  $A_0 = 0$  with  $\mu > 0$  for NUSM. Lighter Higgs boson mass limits are represented by solid lines. Dot-dashed line refers to  $b \rightarrow s\gamma$  limit. WMAP allowed regions are shown by red dots. The  $B_s \rightarrow \mu^+\mu^-$  bound is represented by the long-dashed line and this discards a small strip of region below the discarded top gray region. The small figure within the inset is shown for an improved display of the stau coannihilation zone. (b) Variation of  $\sin(\beta - \alpha)$  vs  $m_0$  for  $m_{1/2} = 500$  GeV,  $\tan \beta = 15$  and  $A_0 = 0$  for NUSM. The figure shows that for large  $m_0$ , actually near the region where  $m_A$  is small,  $\sin(\beta - \alpha)$  is consistently small. This is of course much away from decoupling region of SUSY Higgs boson. The figure in inset shows the finer variation of  $\sin(\beta - \alpha)$  within a small range of  $m_0$ . The gray shaded region refers to the similarly shaded discarded region of Fig.4(a).

effective lower limit.<sup>7</sup>

We have further drawn the  $b \rightarrow s\gamma$  contour by considering a  $3\sigma$  limit [54],

$$2.77 \times 10^{-4} < Br(b \rightarrow s\gamma) < 4.33 \times 10^{-4}. \quad (17)$$

Clearly in Fig.3(a) this constraint would keep the  $m_{1/2} > 425$  GeV region alive and this is indeed the region of super-large  $m_0 \gtrsim 4$  TeV that satisfies the WMAP data. In this context we should however note that the  $b \rightarrow s + \gamma$  constraint may be of less importance if some additional theoretical assumptions are taken into consideration. The computation of the constraint in models like mSUGRA assumes a perfect alignment of the squark and

<sup>7</sup>The following values of top and bottom quarks are considered in the SUSPECT code used in our analysis:  $m_t = 172.7$  GeV and  $m_b^{\overline{MS}}(m_b) = 4.25$  GeV.



quark mass-matrices. This essentially considers an unaltered set of mixing angle factors than the Cabibbo-Kobayashi-Maskawa (CKM) factors at the corresponding SM vertices. Even a small set of off-diagonal terms in squark mass matrices at the unification scale may cause a drastic change in the mixing pattern of the squark sector at the electroweak scale. This however does not cause any effective change in the sparticle mass spectra or in the flavor conserving process of neutralino annihilation or in generating events in a hadron collider in any significant way. A brief review of the model-dependent assumptions for the  $b \rightarrow s\gamma$  analyses may be seen in Refs. ([55], [56]) and references therein.

We now explain an interesting aspect of the NUSM Higgs boson as a consequence of the LSM effect. As we have seen before,  $m_A$  decreases with increasing  $m_0$  in the NUSM. We find that with larger  $m_0$ ,  $m_A$  may become very light for the small  $m_{\frac{1}{2}}$  zone so that we may find a spectrum where  $m_h \sim m_H \sim M_A$  and this indeed is a consequence of moving into the intense-coupling [32] region of Higgs bosons. This results in a change in the value of the coupling  $g_{ZZh} \propto \sin(\beta - \alpha)$ , where  $\alpha$  is the mixing angle between two neutral Higgs bosons  $h$  and  $H$ . Typically in the decoupling region  $\sin(\beta - \alpha)$  stays very close to 1, but in the intense coupling region this can be considerably small like 0.5 or lesser. This effectively reduces the lower limit of  $m_h$  to 93 GeV, a value close to  $m_Z$ . In the NUSM we obtain this effect for a small region of parameter space (small  $m_{\frac{1}{2}}$ ) if  $\tan\beta \gtrsim 15$ . Fig.4(a) shows such a region (this may also satisfy the WMAP limits) for  $200 \text{ GeV} \lesssim m_{\frac{1}{2}} \lesssim 300 \text{ GeV}$  and this appears very close to the top gray shaded discarded zone. Fig.4(b) demonstrates the existence of a small  $\sin(\beta - \alpha)$  in the NUSM as discussed above. However with  $A_0 = 0$ , we will see that such a very light  $m_A$  or  $m_h$  region is almost discarded via the present limit of the  $B_s \rightarrow \mu^+\mu^-$ . The current experimental limit for the  $Br(B_s \rightarrow \mu^+\mu^-)$  coming from CDF [57] puts a strong constraint on the MSSM parameter space. The experimental bound is given by (at 95% C.L.)

$$\text{Br}(B_s \rightarrow \mu^+\mu^-) < 5.8 \times 10^{-8}. \quad (18)$$

The estimate of  $B_s \rightarrow \mu^+\mu^-$  [58] in the MSSM sensitively depends on the mass of A-boson ( $\propto m_A^{-4}$ ) and on the value of  $\tan\beta$  ( $\propto \tan^6\beta$ ).  $B_s \rightarrow \mu^+\mu^-$  constraint eliminates the thin region along the boundary of the REWSB in NUSM where  $m_A$  is very light. As mentioned before, for  $\tan\beta \gtrsim 15$  a part of the above region for small  $m_{\frac{1}{2}}$  zone has non-Standard Model like  $h$ -boson.

Apart from the above constraints we would like to remind that there is no non-universality

in the first two-generations in NUSM. This saves from the stringent FCNC violating limits such as those coming from the  $K_L$ - $K_S$  mass difference or from the  $\mu \rightarrow e\gamma$  bound. Splitting of the first generation and the third generation of scalars may also cause violations of FCNC bounds, although to a lesser extent. Following Ref. [22] we see that for no violation of FCNC one would need (for equal gluino and average squark masses)  $|m_{\bar{q}}(1) - m_{\bar{q}}(3)| \lesssim m_{\bar{q}}^2/M_W$ . Here  $m_{\bar{q}}$  refers to the average squark mass. Considering the analysis performed in Ref. [22] for different gluino masses we conclude that the results of our analysis stay in the safe zone regarding the FCNC bounds in spite of the inter-generational splitting between the squarks. Fig.5(a) shows the results for  $\tan\beta = 40$ . Here the funnel region is extended up to  $m_{1/2} = 1.7$  TeV. A large value of  $\tan\beta$  increases  $h_b$  and  $h_\tau$  and this would enhance the width  $\Gamma_A$  [59]. We point out that unlike Fig.3(a), here the reach of  $m_0$  decreases for a given  $m_{1/2}$ . The mass of A-boson decreases with increase of  $m_0$  much more rapidly because of larger  $h_b$  and  $h_\tau$  arising out of larger values of  $\tan\beta$ . Here, the very light  $m_A$  region that satisfies the WMAP data and that evades the LEP2 Higgs boson limit exists near the top gray boundary for  $250 \text{ GeV} \lesssim m_{\frac{1}{2}} \lesssim 350 \text{ GeV}$  which is again ruled out via the  $B_s \rightarrow \mu^+\mu^-$  limit. The upper gray region is typically discarded here via the REWSB constraint of  $m_A^2$  that turns negative at the tree level. Finally, we have not imposed any limit from the muon  $g - 2$  data that may or may not show a discrepancy from the Standard Model result. It is known that using the recent  $e^+e^-$  data leads to a  $3.4\sigma$  level of discrepancy. On the other hand, using hadronic  $\tau$ -decay data in computing the leading order hadronic contribution to muon  $g - 2$  washes away [60] any deviation from the SM result.

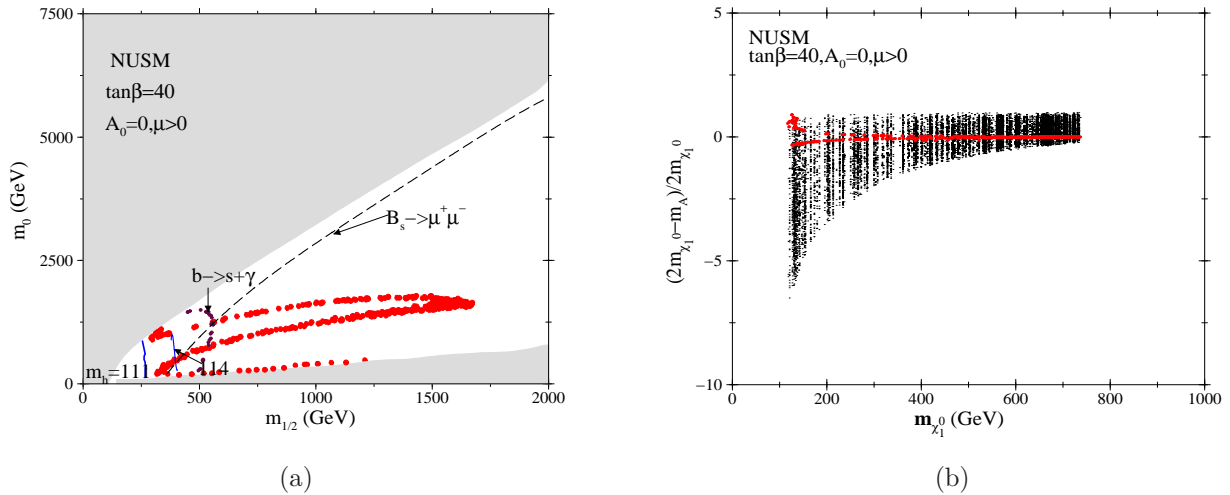


Figure 5: Same as Fig.3 except  $\tan\beta = 40$ .

### 3.1 Sample parameter points satisfying WMAP data for early run of LHC

We would focus on a few characteristic parameter points to discuss the nature of the NUSM spectra that satisfy the WMAP limits. Clearly one is able to reach a considerably large  $m_0$  satisfying dark matter relic density constraints and all other necessary constraints for  $m_{\frac{1}{2}} < 1$  TeV. As an example with  $m_{\frac{1}{2}} = 1$  TeV, this limit is around 7 TeV for  $\tan\beta = 10$ , 6 TeV for  $\tan\beta = 15$ , and 1.6 TeV for  $\tan\beta = 40$ . Thus, for larger  $\tan\beta$  the reach of  $m_0$  decreases considerably. On the other hand, it is not unusual to obtain an  $A$ -pole annihilation region for a large  $\tan\beta$  in popular models like mSUGRA. Hence, if we are interested in focusing on a region of the MSSM that is not available in mSUGRA type of models we would rather explore the smaller  $\tan\beta$  domain of the NUSM. The other important zone of parameter space could be the region with smaller  $m_{\frac{1}{2}}$  because this would be easily accessible in LHC in its early run. We pick up a point on Fig.3(a) (*scenario-A*) that just satisfies the minimum value of  $m_h = 111$  GeV besides being consistent with the WMAP data for cold dark matter. The input parameters are:  $\tan\beta = 10$ ,  $A_0 = 0$ ,  $m_{\frac{1}{2}} = 270$  GeV,  $m_0 = 2050$  GeV and  $sign(\mu) = 1$ . The *scenario-A* of Table 1 thus has light stop and light sbottom quarks, light charginos and neutralinos and at the same time it would have a light Higgs spectra, all of which are promising for an early LHC detection. We remind ourselves that typically the NUSM is associated with a heavy first two-generation of scalars and heavy sleptons for all the three generations. We note that we have relaxed the  $b \rightarrow s\gamma$  constraint keeping in mind of the argument given after Eq.17. We could of course respect the constraint, only at a price of having a little heavier spectra, still that would be very much accessible in LHC for the third generation of squarks, Higgs bosons, charginos etc. This however would not cause any essential change in the general pattern. On the other hand, with not so light  $m_A$  and with a small  $\tan\beta$  the *scenario-A* satisfies the  $B_s \rightarrow \mu^+\mu^-$  limit. The *scenario-B* of Fig.4(a) refers to a special point ( $\tan\beta = 15$ ,  $A_0 = 0$ ,  $m_{\frac{1}{2}} = 255$  GeV,  $m_0 = 2000$  GeV and  $sign(\mu) = 1$ ) for which the Higgs sector is not in the decoupling region thus reducing the limit of  $m_h$  to a value near the  $Z$ -boson mass. This parameter point obeys the  $B_s \rightarrow \mu^+\mu^-$  limit but as with the *scenario-A* it has an inadequate  $Br(b \rightarrow s\gamma)$ . With smaller  $m_{\frac{1}{2}}$  and smaller  $m_0$  *scenario-B* has a lighter spectrum in general than *scenario-A*. Particularly, we find a much smaller Higgs boson spectra. The *scenario-C* (with  $\tan\beta = 40$ ,  $A_0 = 0$ ,  $m_{\frac{1}{2}} = 540$  GeV,  $m_0 = 1250$  GeV and  $sign(\mu) = 1$ ), that satisfy all the constraints including the  $b \rightarrow s\gamma$

bound provides a relatively heavier spectra. This is however still within the LHC reach for the relevant part of the NUSM as mentioned above. We note that the large  $m_0$  domain of the NUSM is typically associated with lighter Higgs spectrum and this region may in general be probed via the production of all MSSM Higgs bosons and subsequently their decays. The squarks corresponding to the first two generations and sleptons of all the generations are large when  $m_0$  is large. As a result the production cross-section of these particles will be too low at the LHC. Thus, to see any SUSY signal for the NUSM one should primarily analyze productions and decays of gluino, stop and sbottom in addition to charginos and neutralinos. In a part of the parameter space where the Higgs spectra is light, all the Higgs states may be produced via  $pp \rightarrow h, H, A, H^\pm + X$  either via loop-induced processes like ( $gg \rightarrow h, H, A$ ) or through cascade decays via heavier charginos and neutralinos  $pp \rightarrow \chi_2^\pm, \chi_3^0, \chi_4^0 \rightarrow \chi_1^\pm, \chi_2^0, \chi_1^0 + h, H, A, H^\pm$ . The latter decays are only allowed if enough phase space is available.

## 4 Direct and Indirect detections of dark matter

### 4.1 Direct detection rates

We will now discuss the prospects of direct and indirect detections [61] of neutralino (LSP) as a candidate for dark matter in the NUSM. First, we will discuss the direct detection of LSP via measurements of nuclear recoil. Neutralinos interact via spin-independent (scalar) and spin-dependent interaction [38, 62] with nucleons. The scalar cross-section may be expressed in terms of number of protons and neutrons,  $Z$  and  $(A - Z)$  respectively [38] as follows.

$$\sigma_{scalar} = 4 \frac{m_r^2}{\pi} [Z f_p + (A - Z) f_n]^2, \quad (19)$$

where  $m_r$  is the reduced LSP mass. The quantities  $f_p$  and  $f_n$  contain all the information of short distance physics and nuclear partonic strengths and these may be seen in Refs. [63]. We will now comment on the relative strengths of spin-independent and spin-dependent neutralino-nuclear cross-sections. While  $\sigma_{scalar}$  depends on  $Z$  and  $A - Z$  quadratically, the spin-dependent interaction cross-section on the other hand is proportional to  $J(J + 1)$  where  $J$  is the total nuclear spin [38]. Typically the spin-independent neutralino-nucleon scattering

parameter	A	B	C
$\tan \beta$	10.0	15.0	40.0
$m_{1/2}$	270.0	255.0	540.0
$m_0$	2050.0	2000.0	1250.0
$A_0$	0	0	0
$sgn(\mu)$	1	1	1
$\mu$	312.60	291.53	651.60
$m_{\tilde{g}}$	709.32	674.43	1278.26
$m_{\tilde{u}_L}$	2103.25	2047.68	1658.64
$m_{\tilde{t}_1}$	276.89	248.27	842.00
$m_{\tilde{t}_2}$	493.53	465.21	1028.15
$m_{\tilde{b}_1}$	390.66	354.64	958.59
$m_{\tilde{b}_2}$	434.06	403.08	1019.74
$m_{\tilde{e}_L}$	2050.19	1999.70	1296.33
$m_{\tilde{\tau}_1}$	2037.46	1972.60	1119.32
$m_{\tilde{\chi}_1^\pm}$	196.44	183.99	430.22
$m_{\tilde{\chi}_2^\pm}$	347.34	327.11	668.46
$m_{\tilde{\chi}_4^0}$	347.72	326.97	668.18
$m_{\tilde{\chi}_3^0}$	318.11	297.66	655.13
$m_{\tilde{\chi}_2^0}$	197.69	185.15	430.30
$m_{\tilde{\chi}_1^0}$	108.05	101.72	226.91
$m_A$	259.48	148.37	403.03
$m_{H^+}$	272.027	169.44	411.73
$m_h$	111.26	111.25	116.32
$\Omega_{\tilde{Z}_1} h^2$	0.105	0.102	0.13
$BF(b \rightarrow s\gamma)$	$1.59 \times 10^{-4}$	$4.65 \times 10^{-5}$	$2.73 \times 10^{-4}$
$BF(B_s \rightarrow \mu^+\mu^-)$	$4.02 \times 10^{-9}$	$2.81 \times 10^{-8}$	$5.29 \times 10^{-8}$
$\Delta a_\mu$	$9.31 \times 10^{-11}$	$1.59 \times 10^{-10}$	$6.99 \times 10^{-10}$

Table 1: Data for point A, B, and C. Masses are in GeV

cross-sections ( where  $\sigma_{\chi p, SI} \simeq \sigma_{\chi n, SI}$ ) are appreciably smaller than the corresponding spin-dependent cross-sections ( $\sigma_{\chi p, SD} \simeq \sigma_{\chi n, SD}$ ). However considering the fact that  $\sigma_{SD} \propto J(J +$

1) and  $\sigma_{SI} \propto Z^2, (A-Z)^2$ ,  $\sigma_{scalar}$  becomes considerably larger for moderately heavy elements ( $A > 30$ ) [3, 64] like Ge, Xe etc. But we should keep in mind that there exists some cases where  $\sigma_{SD}$  may become considerably larger than  $\sigma_{SI}$  even for  $A > 30$ .

The cross-section  $\sigma_{scalar}$  mainly involves the computation of  $\chi - q$  and  $\chi - \tilde{g}$  scattering amplitudes. The scalar cross-section at tree level is composed of  $t$ -channel Higgs boson exchange and  $s$ -channel squark exchange contributions. On the other hand, the spin-dependent cross-section depends on  $t$ -channel  $Z$  exchange and  $s$ -channel squark exchange diagrams. In this analysis we compute the spin-independent cross-section  $\sigma_{scalar}(\tilde{\chi} - p)$  for two values of  $\tan\beta$  (10 and 40) for  $A_0 = 0$  and  $\mu > 0$  using DARKSUSY [65]. Fig. (6) shows  $\sigma_{scalar}(\tilde{\chi} - p)$  vs  $m_{\tilde{\chi}_1^0}$  for  $\tan\beta = 10$  and 40 when  $m_{1/2}$  and  $m_0$  are varied as in Fig.3 and Fig.5 respectively. The WMAP satisfied points are shown in small (maroon) circles. We have shown the limits from CDMS (Ge) 2005 [66], XENON-10 [67] and from future experiments like SuperCDMS (Snolab) [68] and XENON-1T [69]. The neutralinos with higher mass (up to 400 GeV) will be partially probed in XENON-1T while the light LSP region for  $\tan\beta = 40$  is already ruled out by XENON-10 data.

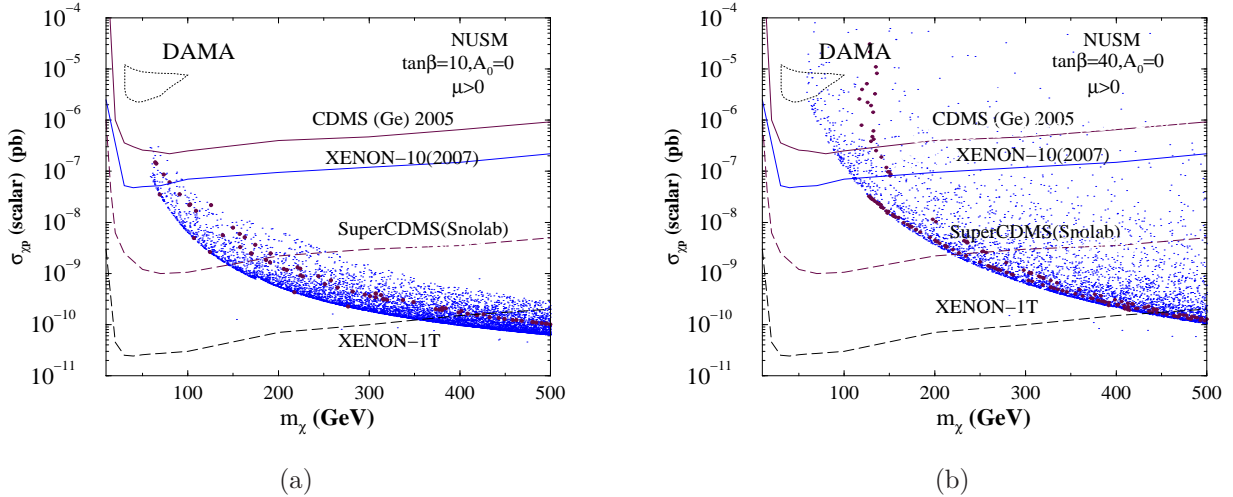


Figure 6: Spin-independent scattering LSP-nucleon cross-sections vs LSP mass for the NUSM for  $\tan\beta = 10$  and 40. The blue dotted region correspond to scanned points of the parameter space of Figs.3 and 5. The maroon filled circles show the WMAP allowed points. Various limit plots are shown for different experiments.

## 4.2 Indirect detection via photon signal

The fact that the A-resonance annihilation is the primary mechanism to satisfy the WMAP limits in the NUSM suggests that there will be enhanced signals for indirect detection via  $\gamma$ -rays, positrons and anti-protons in the NUSM. On the other hand, detection via neutrino signal [61] would not be interesting in this case where the LSP is almost a bino annihilating via A-resonance in the s-channel [59]. Among the above indirect detection possibilities we will limit ourselves to estimating only the detection prospect of gamma rays that originates from the galactic center [70–73]. In general for neutralino annihilation at the galactic center one may have the following possibilities: i) monochromatic  $\gamma$ -rays and ii) continuum  $\gamma$ -rays. Monochromatic  $\gamma$ -rays come out from processes like  $\chi\chi \rightarrow \gamma\gamma$  [74] and  $\chi\chi \rightarrow Z\gamma$  [75]. These signals although small because of the processes being loop suppressed are clean with definite energies  $E_\gamma = m_\chi$  and  $E_\gamma = m_\chi - m_Z^2/4m_\chi$ . Continuum  $\gamma$ -rays on the other hand arise from neutralinos annihilating into a variety of Standard Model particles. The hadronization and production of neutral pions would follow. Typically pion decay, in particular  $\pi^0 \rightarrow \gamma\gamma$  would produce a huge number of photons with varying energies.

The differential continuum  $\gamma$ -ray flux that arrives from angular direction  $\psi$  with respect to the galactic center is given by [61, 71, 72],

$$\frac{d\Phi_\gamma}{dE_\gamma}(E_\gamma, \psi) = \sum_i \frac{\langle \sigma_i v \rangle}{8\pi m_\chi^2} \frac{dN_\gamma^i}{dE_\gamma} \int_{line\ of\ sight} ds \rho_\chi^2(r(s, \psi)). \quad (20)$$

Here  $\sigma_i$  is a LSP pair annihilation cross section into a final channel  $i$ . We will consider  $\gamma$ -rays emerging from the galactic center, hence  $\psi = 0$ .  $v$  is the pair's relative velocity and  $\langle \sigma v \rangle$  refers to the velocity averaged value of  $\sigma v$ .  $\frac{dN_\gamma^i}{dE_\gamma}$  is the differential  $\gamma$ -ray yield for the channel  $i$ .  $\rho_\chi(r)$  is the cold dark matter density at a distance  $r$  from the galactic center, where  $r^2 = s^2 + R_0^2 - 2sR_0 \cos \psi$ . Here,  $s$  is the line of sight coordinate,  $R_0$  is the Solar distance to the galactic center. Clearly,  $\rho_\chi(r)$  that depends on astrophysical modelling is important to determine the photon flux in Eq. (20). One may indeed preferably isolate the right hand side of Eq. (20) into a part depending on particle physics and a part depending on astrophysics. For the later, one defines a dimensionless quantity  $J(\psi)$  such that,

$$J(\psi) = \left( \frac{1}{8.5\text{ kpc}} \right) \left( \frac{1}{0.3\text{ GeV/cm}^3} \right)^2 \int_{line\ of\ sight} ds \rho_\chi^2(r(s, \psi)). \quad (21)$$

The above results in,

$$\frac{d\Phi_\gamma}{dE_\gamma}(E_\gamma, \psi) = 0.94 \times 10^{-13} \text{cm}^{-2} \text{s}^{-1} \text{GeV}^{-1} \text{sr}^{-1} \sum_i \frac{dN_\gamma^i}{dE_\gamma} \left( \frac{\langle \sigma_i v \rangle}{10^{-29} \text{cm}^3 \text{s}^{-1}} \right) \left( \frac{100 \text{ GeV}}{m_\chi} \right)^2 J(\psi). \quad (22)$$

For a detector that has an angular acceptance  $\Delta\Omega$  and lowest energy threshold of  $E_{th}$  the total gamma ray flux from the galactic center is given by,

$$\Phi_\gamma(E_{th}) = 0.94 \times 10^{-13} \text{cm}^{-2} \text{s}^{-1} \sum_i \int_{E_{th}}^{m_\chi} dE_\gamma \frac{dN_\gamma^i}{dE_\gamma} \left( \frac{\langle \sigma_i v \rangle}{10^{-29} \text{cm}^3 \text{s}^{-1}} \right) \left( \frac{100 \text{ GeV}}{m_\chi} \right)^2 \bar{J}(\Delta\Omega) \Delta\Omega. \quad (23)$$

Here  $\bar{J}(\Delta\Omega) = \frac{1}{\Delta\Omega} \int_{\Delta\Omega} J(\psi) d\Omega$ . The upper limit of the integral in Eq.(23) is fixed by the fact that the neutralinos move with galactic velocity, therefore the annihilations may be considered to have occurred at rest. We will now comment on the galactic halo density profiles used in this analysis. Various N-body simulations suggest that one may obtain a general profile behavior arbitrary to the extent of a few parameters and this is given by [76],

$$\rho(r) = \rho_0 \frac{[1 + (R_0/a)^\alpha]^{\frac{(\beta-\gamma)}{\alpha}}}{(r/R_0)^\gamma [1 + (r/a)^\alpha]^{\frac{(\beta-\gamma)}{\alpha}}}. \quad (24)$$

Here  $\rho_0$  is a normalisation factor which is taken as the local (*i.e.* solar region) halo density ( $\simeq 0.3 \text{ GeV}/\text{cm}^3$ ). We will analyze with three popularly used profiles, namely the isothermal cored [77], Navarro, Frenk and White (NFW) profile [78] and Moore profile [79] as given in the Table (2). The table also mentions the corresponding value of  $\bar{J}$  for  $\Delta\Omega = 10^{-3}$  and  $10^{-5}$  sr. Computation of the photon flux for a different halo profile may easily be performed by an appropriate scaling with the corresponding  $\bar{J}$ . Clearly, more cuspy profiles would produce higher photon-flux. One can further include the effects of baryons on the dark matter halo profiles. Baryons may undergo radiative processes leading to a fall towards the central region of a galaxy in formation. This changes the density profiles of matter towards the center which in turn leads to an increased concentration of dark matter. Adiabatic compression [80] has been used to study the baryonic effects. Inclusion of the adiabatic compression effects cause the profiles to become significantly cuspier, often increasing  $\bar{J}$  by a factor of 100 or so [72]. We have not included these halo profile models in our computation, but the photon flux would increase by a similar factor as mentioned above.



Halo Model	$a$ (kpc)	$R_0$ (kpc)	$\alpha$	$\beta$	$\gamma$	$\bar{J}(10^{-3})$	$\bar{J}(10^{-5})$
Isothermal cored	3.5	8.5	2	2	0	30.35	30.4
NFW	20.0	8.0	1	3	1	$1.21 \times 10^3$	$1.26 \times 10^4$
Moore	28.0	8.0	1.5	3	1.5	$1.05 \times 10^5$	$9.75 \times 10^6$

Table 2: A few dark matter halo density profiles and associated parameters.

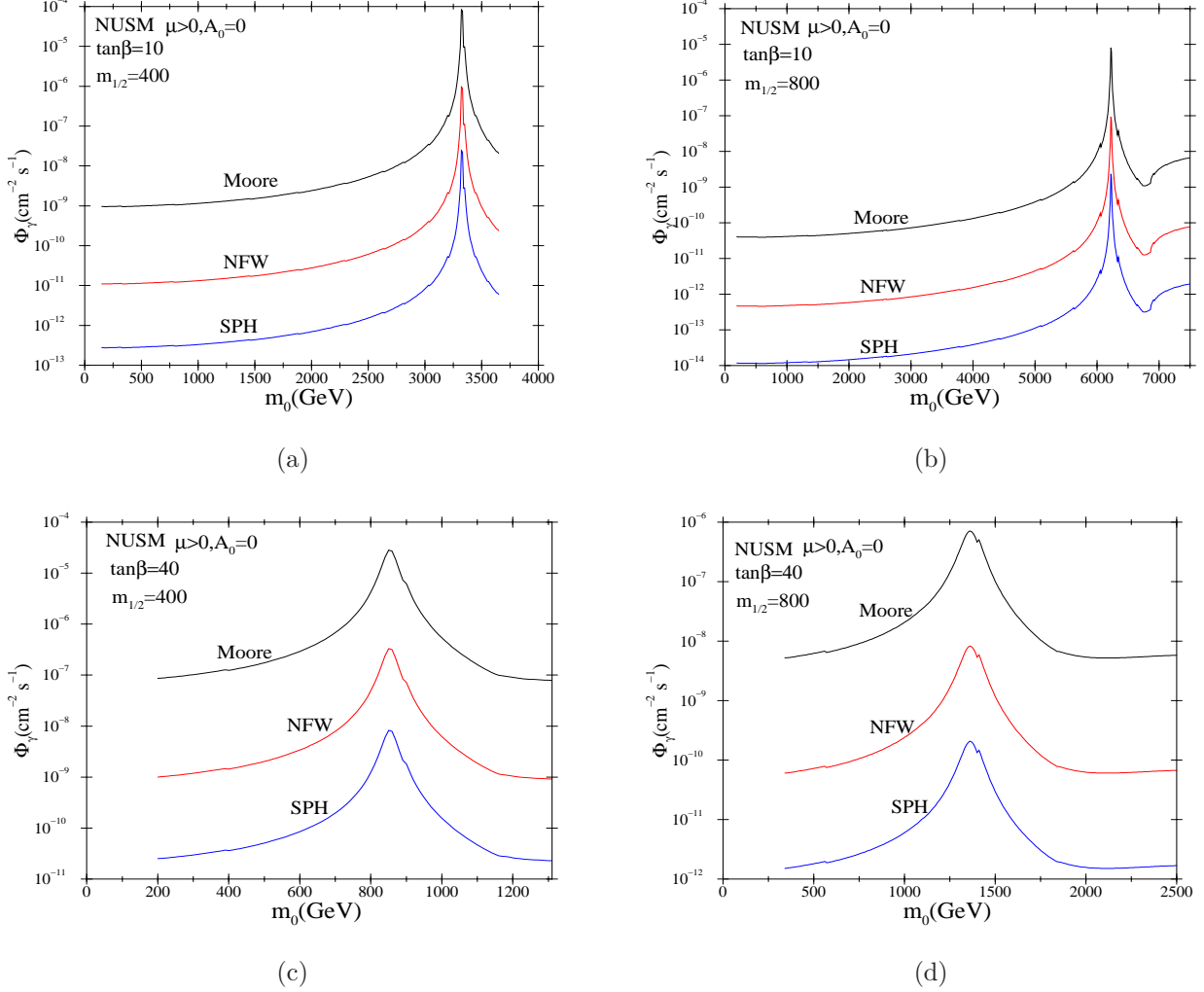


Figure 7: Continuous  $\gamma$ -ray flux in  $\text{cm}^{-2}\text{s}^{-1}$  above a threshold energy of 1 GeV for a cone of  $1 \times 10^{-3}$  sr centered around the galactic center *vs*  $m_0$ . Lines are shown for three different halo distributions i) spherically symmetric isothermal cored profile (SPH) [77], ii) Navarro, Frenk and White (NFW) profile [78] and iii) Moore profile [79].

Fig.(7) shows the result of continuum photon-flux *vs*  $m_0$  for  $\tan\beta = 10$  and 40 corresponding to two different values of  $m_{1/2}$  ( $= 400$  and  $800$  GeV) and three different halo profiles as mentioned above. The photon flux (in  $\text{cm}^{-2}\text{s}^{-1}$ ) in the NUSM is computed using DARK-SUSY [65] with  $E_\gamma > 1$  GeV, for a solid angle aperture of  $\Delta\Omega = 10^{-3}$  sr. As  $m_0$  increases the mass of pseudoscalar Higgs boson decreases and the LSP pair annihilation through s-channel resonance causes a peak corresponding to a halo profile. Broadly, such a peak covers the region of  $m_0$  for a given  $m_{1/2}$  where WMAP data for the neutralino relic density is satisfied. With an increase in  $\tan\beta$  the width  $\Gamma_A$  of  $m_A$  increases and the peak associated with a given halo profile broadens. We see that in spite of having a broad range of halo profile characteristics, the photon flux in the region of resonance annihilation in the NUSM where the WMAP data is satisfied may be probed in the upcoming GLAST [81, 82] experiment at least for the cuspiest profiles. GLAST would be able to probe photon-flux as low as  $10^{-10}$  photons/cm<sup>2</sup>/s [82]. We note that this conclusion remains valid in spite of the fact that GLAST will use an aperture of  $\Delta\Omega = 10^{-5}$  sr so that an appropriate scaling of the photon-flux in Fig.(7) needs to be done from Table (2) and Eq.(23). We further note that as mentioned before, the use of the adiabatic compression mechanism would modify a given halo profile significantly and this may increase the photon flux by a few orders of magnitude. Fig.(8) shows the plots of photon-flux (in  $\text{cm}^{-2}\text{s}^{-1}$  with  $E_\gamma > 1$  GeV) vs the mass of the

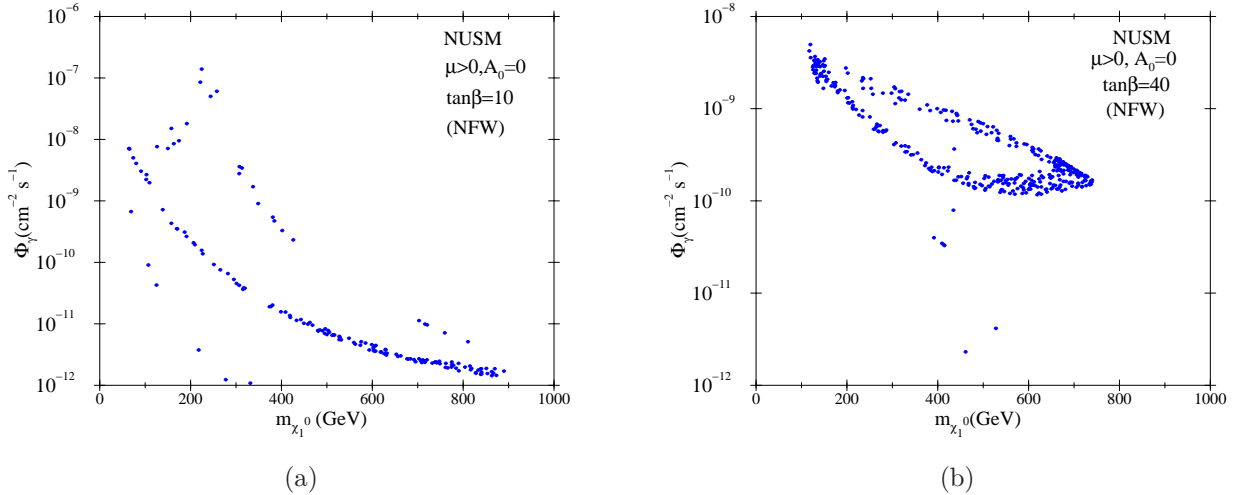


Figure 8: Scatter plot of photon flux in  $\text{cm}^{-2}\text{s}^{-1}$  (with  $E_\gamma > 1$  GeV) vs LSP mass for  $\tan\beta = 10$  and 40 for a NFW halo profile in the NUSM. Here  $m_{1/2}$  and  $m_0$  are scanned in the ranges shown in Figs.(3,5). Only WMAP relic density satisfied points are shown.

LSP for  $\tan\beta = 10$  and 40 for NFW halo profile in the NUSM. Here,  $m_{1/2}$  and  $m_0$  are

varied such that  $m_{1/2} < 2$  TeV and  $m_0 < 20$  TeV for  $\tan\beta = 10$  and  $m_{1/2} < 2$  TeV and  $m_0 < 10$  TeV for  $\tan\beta = 40$ . Only WMAP allowed parameter points are shown. GLAST would be able to probe up to 400 to 450 GeV.

## 5 Conclusion

In this analysis we have worked with a non-universal scalar mass scenario in a supergravity framework. We started with purely phenomenological motivations namely, i) to manage the FCNC and CP-violation type of constraints by decoupling, ii) to obtain WMAP satisfied values for neutralino relic density for a broad region of parameter space without depending on any delicate mixing of gauginos and Higgsinos, iii) to have radiative electroweak symmetry breaking and iv) to keep naturalness within control. Keeping the above in mind and considering a unified gaugino mass scenario, we used a common scalar mass parameter  $m_0$  at the gauge coupling unification scale for the first two-generation of scalars as well as the third generation of sleptons. The item (i) mentioned above would require  $m_0$  to be large, and the item (iv) would prefer light third generation of squarks and light Higgs scalars. For simplicity we used vanishing third generation of squarks and Higgs scalar masses at the unification scale. In such a scenario with a possibly multi-TeV  $m_0$ , we first found a large mass effect or in particular large slepton mass effect in the RGE of  $m_{H_D}^2$  (*ie.* for the down type of Higgs scalar) that turns the later negative at the electroweak scale almost irrespective of a value of  $\tan\beta$ . Extending the semi-analytic solution of  $m_A^2$  by considering the  $h_b$  and the  $h_\tau$  terms (this is required here even for a small  $\tan\beta$ ) relevant for the large slepton mass effect we found a hyperbolic branch/focus point like effect in  $m_A^2$  ( $\simeq m_{H_D}^2 - m_{H_U}^2$ ) for small  $\tan\beta$ . This causes  $m_A$  to be almost independent of  $m_0$  for a large domain of the later. But, with a very large  $m_0$  this causes  $m_A$  to become very light or this may even turn  $m_A^2$  negative giving rise to no radiative electroweak symmetry breaking. We further found that because of such large slepton mass effect in the RGE, the Higgs sector may reach an intense coupling region with all the Higgs bosons becoming very light and this may evade the LEP2 limit of  $m_h$  for a limited region of parameter space. However, constraint from  $Br(B_s \rightarrow \mu^+\mu^-)$  becomes stringent in this region because of lighter  $m_A$ . In general, we find relatively lighter  $m_A$  or  $m_H$  and this fact leads to a large  $A$ -pole annihilation region or funnel region of dark matter even for a small  $\tan\beta$ . This is in contrast to minimal supergravity type of scenar-

ios where funnel region may occur only for large values of  $\tan\beta$ . The nature of the LSP is bino-dominated, thus there is no need of any delicate mixing of binos and Higgsinos in order to satisfy the neutralino relic density constraint. We have also computed the direct detection rates of LSP-nucleon scattering. The upcoming detectors like XENON-1T would be able to probe almost the entire region of parameter space. We have further estimated the indirect detection prospect via computing continuous photon fluxes. The ongoing GLAST experiment will be successfully able to probe the parameter space even for a less cuspy halo profile. We have also briefly discussed the detection prospect of sparticles in the LHC. The Higgs bosons and the third generation of squarks are light in this scenario. In addition to charginos and neutralinos the above may be easily probed in the early runs of LHC.

## 6 Appendix

The coefficients appearing in Eqs. 7 and 8 are given by,

$$C_2 = \frac{\tan^2\beta}{(\tan^2\beta - 1)}k, \quad C_3 = -\frac{1}{(\tan^2\beta - 1)}(g - e \tan^2\beta), \quad \text{and } C_4 = -\frac{\tan^2\beta}{(\tan^2\beta - 1)}f \quad (25)$$

$$D_2 = \frac{\tan^2\beta + 1}{\tan^2\beta - 1}k, \quad D_3 = -\frac{\tan^2\beta + 1}{\tan^2\beta - 1}(g - e), \quad \text{and } D_4 = -\frac{\tan^2\beta + 1}{\tan^2\beta - 1}f \quad (26)$$

Here the functions  $k, g, e$  and  $f$  may be seen in Ref. [35]. Electroweak scale result of  $Y_i = h_i^2/(4\pi)^2$  with  $i \equiv t, b$ , and  $\tau$  are shown below.

$$Y_1(t) = \frac{E_1(t)Y_1(0)}{1 + 6Y_1(0)F(t)}, \quad Y_2(t) = \frac{E_2(t)Y_2(0)}{(1 + 6Y_1(0)F(t))^{\frac{1}{6}}}, \quad \text{and } Y_3(t) = Y_3(0)E_3(t) \quad (27)$$

The quantities  $E_i(t)$  are defined as follows.

$$\begin{aligned} E_1(t) &= (1 + \beta_3(t))^{\frac{16}{3b_3}} (1 + \beta_2(t))^{\frac{3}{b_2}} (1 + \beta_1(t))^{\frac{13}{9b_1}} \\ E_2(t) &= (1 + \beta_1(t))^{\frac{-2}{3b_1}} E_1(t) \\ E_3(t) &= (1 + \beta_1(t))^{\frac{3}{b_1}} (1 + \beta_2(t))^{\frac{3}{b_2}} \end{aligned} \quad (28)$$

Here,  $F(t) = \int_0^t E_1(t')dt'$ ,  $\beta_i = \alpha_i(0)b_i/4\pi$  and  $(b_1, b_2, b_3) = (33/5, 1, -3)$ .

### Acknowledgments

DD would like to thank the Council of Scientific and Industrial Research, Govt. of India

for the support received as a Junior Research Fellow. UC is thankful to the organizers of the workshop “TeV Scale and Dark Matter (2008)” at NORDITA where the last part of the work was completed. UC acknowledges useful discussions with M. Guchait, A. Kundu, B. Mukhopadhyaya, D. Choudhury, D.P. Roy, Jan Kalinowski and S. Roy.

## References

- [1] For reviews on Supersymmetry, see, *eg*, H. P. Nilles, Phys. Rep. **110**, 1 (1984); H. E. Haber and G. Kane, Phys. Rep. **117**, 75 (1985) ; J. Wess and J. Bagger, *Supersymmetry and Supergravity*, 2nd ed., (Princeton, 1991); M. Drees, P. Roy and R. M. Godbole, *Theory and Phenomenology of Sparticles*, (World Scientific, Singapore, 2005).
- [2] T. P. Cheng and L. F. Li, *Oxford, UK: Clarendon ( 1984) 536 P. ( Oxford Science Publications)*
- [3] D. J. H. Chung, L. L. Everett, G. L. Kane, S. F. King, J. D. Lykken and L. T. Wang, Phys. Rept. **407**, 1 (2005); S. P. Martin, arXiv:hep-ph/9709356.
- [4] A. H. Chamseddine, R. Arnowitt and P. Nath, Phys. Rev. Lett. **49**, 970 (1982); R. Barbieri, S. Ferrara and C. A. Savoy, Phys. Lett. B **119**, 343 (1982); L. J. Hall, J. Lykken and S. Weinberg, Phys. Rev. D **27**, 2359 (1983); P. Nath, R. Arnowitt and A. H. Chamseddine, Nucl. Phys. B **227**, 121 (1983); N. Ohta, Prog. Theor. Phys. **70**, 542 (1983); For reviews see [1] and P. Nath, R. Arnowitt and A.H. Chamseddine, *Applied N =1 Supergravity* (World Scientific, Singapore, 1984).
- [5] V. Berezhinsky, A. Bottino, J. Ellis, N. Forrengo, G. Mignola, and S. Scopel, *Astropart. Phys.*5:1-26(1996).
- [6] P. Nath and R. Arnowitt, Phys. Rev. D **56**, 2820 (1997)
- [7] D. G. Cerdeno and C. Munoz, *JHEP* **0410**, 015 (2004) [arXiv:hep-ph/0405057].
- [8] J. Ellis, K. A. Olive and P. Sandick, arXiv:0805.2343 [hep-ph]; J. R. Ellis, K. A. Olive, Y. Santoso and V. C. Spanos, Phys. Lett. B **603**, 51 (2004); J. R. Ellis, T. Falk, K. A. Olive and Y. Santoso, Nucl. Phys. B **652**, 259 (2003) [arXiv:hep-ph/0210205];

- A. De Roeck, J. R. Ellis, F. Gianotti, F. Moortgat, K. A. Olive and L. Pape, *Eur. Phys. J. C* **49**, 1041 (2007) [arXiv:hep-ph/0508198].
- [9] H. Baer, A. Mustafayev, E. K. Park and X. Tata, *JHEP* **0805**, 058 (2008);  
H. Baer, A. Mustafayev, E. K. Park, S. Profumo and X. Tata, *JHEP* **0604**, 041 (2006);  
S. Bhattacharya, A. Datta and B. Mukhopadhyaya, arXiv:0804.4051 [hep-ph]; S. Bhattacharya, A. Datta and B. Mukhopadhyaya, arXiv:0809.2012 [hep-ph];
- [10] H. Baer, A. Mustafayev, S. Profumo, A. Belyaev and X. Tata, *JHEP* **0507**, 065 (2005);  
H. Baer, A. Mustafayev, S. Profumo, A. Belyaev and X. Tata, *Phys. Rev. D* **71**, 095008 (2005).
- [11] U. Chattopadhyay, D. Choudhury and D. Das, *Phys. Rev. D* **72**, 095015 (2005); U. Chattopadhyay and D. P. Roy, *Phys. Rev. D* **68**, 033010 (2003); A. Corsetti and P. Nath, *Phys. Rev. D* **64**, 125010 (2001); U. Chattopadhyay, A. Corsetti and P. Nath, *Phys. Rev. D* **66**, 035003 (2002); U. Chattopadhyay and P. Nath, *Phys. Rev. D* **65**, 075009 (2002); S. Bhattacharya, A. Datta and B. Mukhopadhyaya, *JHEP* **0710**, 080 (2007); S. Bhattacharya, A. Datta and B. Mukhopadhyaya, arXiv:0804.4051 [hep-ph]; K. Huitu, J. Laamanen, P. N. Pandita and S. Roy, *Phys. Rev. D* **72**, 055013 (2005); K. Huitu, R. Kinnunen, J. Laamanen, S. Lehti, S. Roy and T. Salminen, arXiv:0808.3094 [hep-ph]; S. F. King, J. P. Roberts and D. P. Roy, *JHEP* **0710**, 106 (2007) [arXiv:0705.4219 [hep-ph]]; G. Belanger, F. Boudjema, A. Cottrant, A. Pukhov and A. Semenov, *Nucl. Phys. B* **706**, 411 (2005) [arXiv:hep-ph/0407218].
- [12] S. K. Soni and H. A. Weldon, *Phys. Lett.* **B126**, 215(1983); V. S. Kaplunovsky and J. Louis, *Phys. Lett.* **B306**, 269(1993).
- [13] M. Dine, R. Leigh, and A. Kagan, *Phys. Rev.* **D48**, 4269 (1993); P. Pouliot and N. Seiberg, *Phys. Lett.* **B318**, 169 (1993); Y. Nir and N. Seiberg, *Phys. Lett.* **B309**, 337 (1993). S. Dimopoulos and G.F. Giudice, *Phys. Lett.* **B357**, 573 (1995); A. Cohen, D.B. Kaplan, and A.E. Nelson, *Phys. Lett.* **B388**, 588 (1996); M. Misiak, S. Pokorski and J. Rosiek, *Adv. Ser. Direct. High Energy Phys.* **15**, 795 (1998) [arXiv:hep-ph/9703442]; P. H. Chankowski, K. Kowalska, S. Lavignac and S. Pokorski, arXiv:hep-ph/0507133.
- [14] N. Arkani-Hamed and H. Murayama, *Phys. Rev. D* **56**, R6733 (1997) [arXiv:hep-ph/9703259].

- [15] F. Gabbiani, E. Gabrielli, A. Masiero and L. Silvestrini, Nucl. Phys. B **477**, 321 (1996) [arXiv:hep-ph/9604387].
- [16] R. Barbieri and G.F. Giudice, Nucl. Phys. **B306**,63(1988); P. Ciafaloni and A. Strumia, Nucl. Phys. **B494**, 41(1997); G. Bhattacharya and A. Romanino, Phys. Rev. **D55**, 7015(1997).
- [17] J. Bagger, J. L. Feng and N. Polonsky, Nucl. Phys. B **563**, 3 (1999); . K. Agashe and M. Graesser, Phys. Rev. D **59**, 015007 (1998); J. A. Bagger, J. L. Feng, N. Polonsky and R. J. Zhang, Phys. Lett. B **473**, 264 (2000).
- [18] H. Baer, C. Balazs, P. Mercadante, X. Tata and Y. Wang, Phys. Rev. D **63**, 015011 (2000) [arXiv:hep-ph/0008061].
- [19] J. L. Feng, K. T. Matchev and T. Moroi, Phys. Rev. D **61**, 075005 (2000); Phys. Rev. Lett. **84**, 2322 (2000); J. L. Feng, K. T. Matchev and F. Wilczek, Phys. Lett. B **482**, 388 (2000); J. L. Feng and F. Wilczek, Phys. Lett. B **631**, 170 (2005); U. Chattopadhyay, T. Ibrahim and D. P. Roy, Phys. Rev. D **64**, 013004 (2001); U. Chattopadhyay, A. Datta, A. Datta, A. Datta and D. P. Roy, Phys. Lett. B **493**, 127 (2000); S. P. Das, A. Datta, M. Guchait, M. Maity and S. Mukherjee, Eur. Phys. J. C **54**, 645 (2008), [arXiv:0708.2048 [hep-ph]].
- [20] K. L. Chan, U. Chattopadhyay and P. Nath, Phys. Rev. D **58**, 096004 (1998); [arXiv:hep-ph/9710473]; U. Chattopadhyay, A. Corsetti and P. Nath, Phys. Rev. D **68**, 035005 (2003) [arXiv:hep-ph/0303201];  
See also: 1st article of Ref. [39].
- [21] V. D. Barger, C. Kao and R. J. Zhang, Phys. Lett. B **483**, 184 (2000) [arXiv:hep-ph/9911510].
- [22] H. Baer, A. Belyaev, T. Krupovnickas and A. Mustafayev, JHEP **0406**, 044 (2004) [arXiv:hep-ph/0403214].
- [23] S. F. King and J. P. Roberts, JHEP **0609**, 036 (2006);
- [24] D. G. Cerdeno, S. Khalil and C. Munoz, arXiv:hep-ph/0105180.

- [25] N. Arkani-Hamed, A. Delgado and G. F. Giudice, Nucl. Phys. B **741**, 108 (2006), [arXiv:hep-ph/0601041].
- [26] C. D. McMullen and S. Nandi, Phys. Rev. D **75**, 095001 (2007)
- [27] D. Feldman, Z. Liu and P. Nath, JHEP **0804**, 054 (2008); D. Feldman, Z. Liu and P. Nath, Phys. Rev. Lett. **99**, 251802 (2007) [Erratum-ibid. **100**, 069902 (2008)].
- [28] L. Randall and R. Sundrum, Nucl. Phys. **B557**(1999) 79. G.F. Giudice, M.A. Luty, H. Murayama, and R. Rattazzi, J. High Energy Phys. **9812**, 027 (1998); T. Gherghetta, G.F. Giudice, and J.D. Wells, Nucl. Phys. **B559** (1999) 27.
- [29] A. Brignole, L. E. Ibanez and C. Munoz, Nucl. Phys. B **422**, 125 (1994) [Erratum-ibid. B **436**, 747 (1995)] L. E. Ibanez, D. Lust and G. G. Ross, Phys. Lett. B **272**, 251 (1991).
- [30] D. G. Cerdeno, T. Kobayashi and C. Munoz, arXiv:0709.0858 [hep-ph].
- [31] H.E. Haber and Y. Nir, Phys. Lett. **B306** 327 (1993); H.E. Haber, hep-ph/9505240; A. Dobado, M.J. Herrero and S. Penaranda, Eur. Phys. J. **C17** 487 (2000) ; J.F. Gunion and H.E. Haber, Phys. Rev. **D67** 075019 (2003).
- [32] A. Djouadi and Y. Mambrini, JHEP **0612**, 001 (2006); E. Boos, V. Bunichev, A. Djouadi and H.J. Schreiber, Phys. Lett. **B622** 311 (2005); E. Boos, A. Djouadi and A. Nikitenko, Phys. Lett. **B578**, 384 (2004); E. Boos, A. Djouadi, M. Muhlleitner and A. Vologdin, Phys. Rev. **D66** 055004 (2002).
- [33] R. Arnowitt and P. Nath, Phys. Rev. D **46**, 3981 (1992).
- [34] G. Gamberini, G. Ridolfi and F. Zwirner, Nucl. Phys. B **331**, 331 (1990); V. D. Barger, M. S. Berger and P. Ohmann, Phys. Rev. D **49**, 4908 (1994); For two-loop effective potential see: S. P. Martin, Phys. Rev. D **66**, 096001 (2002).
- [35] L. E. Ibanez, C. Lopez and C. Munoz, Nucl. Phys. B **256**, 218 (1985); L. E. Ibanez and C. Lopez Nucl. Phys. B **233**, 511 (1984).
- [36] A. Djouadi, J. L. Kneur and G. Moultaka, arXiv:hep-ph/0211331.
- [37] J. R. Ellis, K. A. Olive and P. Sandick, Phys. Lett. B **642**, 389 (2006) [arXiv:hep-ph/0607002].



- [38] G. Jungman, M. Kamionkowski and K. Greist, Phys. Rep. **267**, 195 (1996).
- [39] A. B. Lahanas, N. E. Mavromatos and D. V. Nanopoulos, Int. J. Mod. Phys. D **12**, 1529 (2003) [arXiv:hep-ph/0308251]; C. Munoz, Int. J. Mod. Phys. A **19**, 3093 (2004) [arXiv:hep-ph/0309346]; Manuel Drees, Plenary talk at 11th International Symposium on Particles, Strings and Cosmology (PASCOS 2005), Gyeongju, Korea, 30 May - 4 Jun 2005 (published in AIP Conf.Proc., **805**, 48-54, (2006)).
- [40] E. Komatsu *et al.* [WMAP Collaboration], arXiv:0803.0547 [astro-ph].
- [41] J. R. Ellis, T. Falk and K. A. Olive, Phys. Lett. B **444**, 367 (1998); J. R. Ellis, T. Falk, K. A. Olive and M. Srednicki, Astropart. Phys. **13**, 181 (2000) [Erratum-ibid. **15**, 413 (2001)]; A. Lahanas, D. V. Nanopoulos and V. Spanos, Phys. Rev. D **62**, 023515 (2000); R. Arnowitt, B. Dutta and Y. Santoso, Nucl. Phys. B **606**, 59(2001); T. Nihei, L. Roszkowski and R. Ruiz de Austri, JHEP **0207**, 024 (2002); V. A. Bednyakov, H. V. Klapdor-Kleingrothaus and V. Gronewold, Phys. Rev. D **66**, 115005 (2002).
- [42] C. Boehm, A. Djouadi and Manuel Drees, Phys. Rev. D **62**, 035012(2000); J. R. Ellis, K. A. Olive and Y. Santoso, Astropart. Phys. **18**, 395 (2003);  
See also Ref. [48].
- [43] J. Edsjo and P. Gondolo, Phys. Rev. D **56**, 1879 (1997).
- [44] S. Mizuta and M. Yamaguchi, Phys. Lett. B **298**, 120 (1993) [arXiv:hep-ph/9208251].
- [45] R. Arnowitt, B. Dutta and Y. Santoso, Nucl. Phys. B **606**, 59 (2001); V. A. Bednyakov, H. V. Klapdor-Kleingrothaus and V. Gronewold, arXiv:hep-ph/0208178.
- [46] For the latest limits on the sparticle masses from LEP experiments: see <http://lepsusy.web.cern.ch/lepsusy/>
- [47] R. Barate *et al.* [LEP Working Group for Higgs boson searches], Phys. Lett. B **565**, 61 (2003) [arXiv:hep-ex/0306033].
- [48] U. Chattopadhyay, D. Das, A. Datta and S. Poddar, Phys. Rev. D **76**, 055008 (2007) [arXiv:0705.0921 [hep-ph]]; N. Bhattacharyya, A. Datta and S. Poddar, arXiv:0807.0278 [hep-ph].

- [49] M. Drees and M. Nojiri, Phys. Rev. **D47**, 376 (1993).
- [50] R. Arnowitt and P. Nath, Phys. Rev. Lett. **70**, 3696 (1993); H. Baer and M. Brhlik, Phys. Rev. **D53**, 597 (1996), Phys. Rev. D **57**, 567 (1998); H. Baer, M. Brhlik, M. Diaz, J. Ferrandis, P. Mercadante, P. Quintana and X. Tata, Phys. Rev. **D63**, 015007 (2000); J. R. Ellis, T. Falk, G. Ganis, K. A. Olive and M. Srednicki, Phys. Lett. B **510**, 236 (2001); A. B. Lahanas and V. C. Spanos, Eur. Phys. J. C **23**, 185 (2002); A. Djouadi, M. Drees and J. Kneur, Phys. Lett. B **624** 60 (2005).
- [51] G. Belanger, F. Boudjema, A. Pukhov and A. Semenov, Comput. Phys. Commun. **176**, 367 (2007) [arXiv:hep-ph/0607059].
- [52] J. M. Frere, D. R. T. Jones and S. Raby, Nucl. Phys. B **222**, 11 (1983); J. A. Casas, A. Lleyda and C. Munoz, Nucl. Phys. B **471**, 3 (1996) [arXiv:hep-ph/9507294].
- [53] S. Heinemeyer, W. Hollik and G. Weiglein, Phys. Rep. **425**, 265 (2006); S. Heinemeyer, hep-ph/0408340; S. Heinemeyer, Int. J. Mod. Phys. A **21**, 2659 (2006); G. Degrassi, S. Heinemeyer, W. Hollik, P. Slavich and G. Weiglein, Eur. Phys. J. C **28**, 133 (2003); B. C. Allanach, A. Djouadi, J. L. Kneur, W. Porod and P. Slavich, JHEP **0409**, 044 (2004).
- [54] S. Chen, et al., CLEO Collaboration, Phys. Rev. Lett. **87**, 251807 (2001), hep-ex/0108032; P. Koppenburg *et al.* [Belle Collaboration], Phys. Rev. Lett. **93**, 061803 (2004) B. Aubert, et al., BaBar Collaboration, hep-ex/0207076.
- [55] K. i. Okumura and L. Roszkowski, Phys. Rev. Lett. **92**, 161801 (2004); M. E. Gomez, T. Ibrahim, P. Nath and S. Skadhauge, Phys. Rev. D **74**, 015015 (2006).
- [56] A. Djouadi, M. Drees and J. L. Kneur, JHEP **0603**, 033 (2006).
- [57] T. Aaltonen *et al.* [CDF Collaboration], Phys. Rev. Lett. **100**, 101802 (2008).
- [58] J.R. Ellis, K.A. Olive and V.C. Spanos, Phys. Lett. B **624**, 47 (2005); T. Ibrahim and P. Nath, Phys. Rev. D **67**, 016005 (2003); S. Baek, P. Ko, and W. Y. Song, JHEP **0303**, 054 (2003); J. K. Mizukoshi, X. Tata and Y. Wang, Phys. Rev. D **66**, 115003 (2002); R. Arnowitt, B. Dutta, T. Kamon and M. Tanaka, Phys. Lett. B **538** (2002) 121; A. Dedes, H. K. Dreiner, U. Nierste, and P. Richardson, Phys. Rev. Lett. **87**, 251804

- (2001); K. S. Babu and C. Kolda, Phys. Rev. Lett. **84**, 228 (2000); S. R. Choudhury and N. Gaur, Phys. Lett. B **451**, 86 (1999).
- [59] H. Baer, A. Belyaev, T. Krupovnickas and J. O’Farrill, JCAP **0408**, 005 (2004); H. Baer and J. O’Farrill, JCAP **0404**, 005 (2004).
- [60] M. Passera, W. J. Marciano and A. Sirlin, Phys. Rev. D **78**, 013009 (2008).
- [61] G. Bertone, D. Hooper and J. Silk, Phys. Rept. **405**, 279 (2005); G. Bertone and D. Merritt, Mod. Phys. Lett. A **20**, 1021 (2005); J. Carr, G. Lamanna and J. Lavalley, Rept. Prog. Phys. **69**, 2475 (2006).
- [62] M. W. Goodman and E. Witten, Phys. Rev. D **31**, 3059 (1985); K. Greist, Phys. Rev. **D38**, 2357(1988); J. Ellis and R. Flores, Nucl. Phys. **B307**, 883(1988); R. Barbieri, M. Frigeni and G. Giudice, Nucl. Phys. **B313**, 725(1989); A. Bottino et.al., Phys. Lett. **B295**, 330(1992); M. Drees and M.M. Nojiri, Phys. Rev.**D48**,3483(1993); J. R. Ellis, A. Ferstl and K. A. Olive, Phys. Lett. B **481**, 304 (2000); J. D. Vergados, Lect. Notes Phys. **720**, 69 (2007); V. K. Oikonomou, J. D. Vergados and C. C. Moustakidis, Nucl. Phys. B **773**, 19 (2007); J. Ellis, K. A. Olive and C. Savage, Phys. Rev. D **77**, 065026 (2008); D. Feldman, Z. Liu and P. Nath, Phys. Lett. B **662**, 190 (2008); D. Feldman, Z. Liu and P. Nath, arXiv:0808.1595 [hep-ph].
- [63] M. Drees and M. Nojiri, Phys. Rev. **D47**, 4226 (1993) and Phys. Rev. **D48**, 3483 (1993); M. A. Shifman, A. I. Vainshtein and V. I. Zakharov, Phys. Lett. **78B**, 443 (1978); A. I. Vainshtein, V. I. Zakharov and M. A. Shifman, Usp. Fiz. Nauk **131**, 537 (1980).
- [64] V. A. Bednyakov, H. V. Klapdor-Kleingrothaus and S. Kovalenko, Phys. Rev. D **50**, 7128 (1994) [arXiv:hep-ph/9401262].
- [65] P. Gondolo, J. Edsjo, P. Ullio, L. Bergstrom, M. Schelke and E. A. Baltz, JCAP **0407**, 008 (2004) [arXiv:astro-ph/0406204].
- [66] D. S. Akerib *et al.* [CDMS Collaboration], Phys. Rev. Lett. **96**, 011302 (2006) [arXiv:astro-ph/0509259]
- [67] J. Angle *et al.* [XENON Collaboration], Phys. Rev. Lett. **100**, 021303 (2008) [arXiv:0706.0039 [astro-ph]].

- [68] [http://www.fermilabtoday.com/directorate/program\\_planning/March2007PACPublic/CabreraPAC03\\_07.pdf](http://www.fermilabtoday.com/directorate/program_planning/March2007PACPublic/CabreraPAC03_07.pdf);  
For a limit plot see: <http://dendera.berkeley.edu/plotter/entryform.html>
- [69] [http://www.lngs.infn.it/lngs\\_infn/contents/lngs\\_en/research/experiments\\_scientific\\_info/experiments/current/xenon/collaboration.htm](http://www.lngs.infn.it/lngs_infn/contents/lngs_en/research/experiments_scientific_info/experiments/current/xenon/collaboration.htm);  
For a limit plot see : <http://dendera.berkeley.edu/plotter/entryform.html>
- [70] A. Bouquet, P. Salati and J. Silk, Phys. Rev. D **40**, 3168 (1989); F. W. Stecker, Phys. Lett. B **201**, 529 (1988); M. Urban, A. Bouquet, B. Degrange, P. Fleury, J. Kaplan, A. L. Melchior and E. Pare, Phys. Lett. B **293**, 149 (1992); V. S. Berezinsky, A. V. Gurevich and K. P. Zybin, Phys. Lett. B **294**, 221 (1992); V. Berezinsky, A. Bottino and G. Mignola, Phys. Lett. B **325**, 136 (1994); G. Bertone, G. Sigl and J. Silk, Mon. Not. Roy. Astron. Soc. **337**, 98 (2002) [arXiv:astro-ph/0203488]; T. Bringmann, L. Bergstrom and J. Edsjo, JHEP **0801**, 049 (2008).
- [71] L. Bergstrom, P. Ullio and J. H. Buckley, Astropart. Phys. **9**, 137 (1998) [arXiv:astro-ph/9712318].
- [72] Y. Mambrini, C. Munoz, E. Nezri and F. Prada, JCAP **0601**, 010 (2006); Y. Mambrini, C. Munoz and E. Nezri, JCAP **0612**, 003 (2006); L. Roszkowski, R. R. de Austri, J. Silk and R. Trotta, arXiv:0707.0622 [astro-ph]; S. Profumo and A. Provenza, JCAP **0612**, 019 (2006); H. Baer, A. Mustafayev, E. K. Park and S. Profumo, JHEP **0507**, 046 (2005);
- [73] S. Dodelson, D. Hooper and P. D. Serpico, Phys. Rev. D **77**, 063512 (2008); D. Hooper, G. Zaharijas, D. P. Finkbeiner and G. Dobler, Phys. Rev. D **77**, 043511 (2008); D. Hooper and E. A. Baltz, arXiv:0802.0702 [hep-ph]; N. Bernal, A. Goudelis, Y. Mambrini and C. Munoz, arXiv:0804.1976 [hep-ph]; A. Birkedal, K. T. Matchev, M. Perelstein and A. Spray, arXiv:hep-ph/0507194;
- [74] L. Bergstrom and P. Ullio, ‘Full one-loop calculation of neutralino annihilation into two photons’, *Nucl. Phys.* **B504**, 27 (1997); Z. Bern P. Gondolo and M. Perelstein, ‘Neutralino annihilation into two photons’, *Phys. Lett.* **B411**, 86 (1997); U. Chattopadhyay, D. Das, P. Konar and D. P. Roy, Phys. Rev. D **75**, 073014 (2007); U. Chattopadhyay, D. Choudhury, M. Drees, P. Konar and D. P. Roy, Phys. Lett. B **632**, 114 (2006).

- [75] P. Ullio and L. Bergstrom, Phys. Rev. D **57**, 1962 (1998) [arXiv:hep-ph/9707333].
- [76] L. Hernquist, Astrophys. J. **356**, 359 (1990).
- [77] J. Binney and S. Tremaine, *Galactic Dynamics*, (Princeton University Press, Princeton, 1987).
- [78] J.F. Navarro, C.S. Frenk, S.D.M. White, Astrophys. J. 462 (1996) 563; J.F. Navarro, C.S. Frenk, S.D.M. White, Astrophys. J. 490 (1997) 493.
- [79] B. Moore, T. Quinn, F. Governato, J. Stadel and G. Lake, Mon. Not. Roy. Astron. Soc. **310**, 1147 (1999) [arXiv:astro-ph/9903164].
- [80] G. R. Blumenthal, S. M. Faber, R. Flores and J. R. Primack, Astrophys. J. **301**, 27 (1986); R. Jesseit, T. Naab and A. Burkert, Astrophys. J. Lett **571**, L89 (2002), arXiv:astro-ph/0204164; O. Y. Gnedin, A. V. Kravtsov, A. A. Klypin and D. Nagai, Astrophys. J. **616**, 16 (2004) [arXiv:astro-ph/0406247]; F. Prada, A. Klypin, J. Flix, M. Martinez and E. Simonneau, arXiv:astro-ph/0401512;
- [81] The gamma-ray large area space telescope (GLAST): <http://glast.gsfc.nasa.gov>;
- [82] A. Morselli, A. Lionetto, A. Cesarini, F. Fucito and P. Ullio [GLAST Collaboration], Nucl. Phys. Proc. Suppl. **113**, 213 (2002) [arXiv:astro-ph/0211327].